FINAL REPORT

Development and Evaluation of a Hydrogen Fuel Power Plant for a Hybrid Electric Vehicle — Phase II

Submitted to the
South Coast Air Quality Management District
Contract 95073, Project 7

December, 1997

by :
Joseph M. Norbeck, Principal Investigator
Matthew J. Barth, Co-Investigator
Jay A. Farrell, Co-Investigator
James W. Heffel, Project Manager

University of California
College of Engineering
Center for Environmental Research and Technology
Riverside, CA 92521-0434

97-AV-RT66-004-FR

THIS REPORT WAS PRODUCED UNDER FUNDING FROM THE SOUTH COAST AIR QUALITY MANAGEMENT DISTRICT

DELIVERABLE TECHNICAL SUMMARY FOR CONTRACT NO. 95073, PROJECT 7

Acknowledgments

CE-CERT gratefully acknowledges the support of the South Coast Air Quality Management District in sponsoring this project. BKM, Inc., provided the fuel injectors and technical data. Michael McClanahan and Tim Fleenor set up tests and managed implementation. UC Riverside students Anthony Rossi, Forrest Jehlik, Ryan Gross, and Tony Givargis assisted in the experiments and compiling the report. This report was written at CE-CERT by Jay Farrell, James Harvey, Matthew Barth, James Heffel, and Anthony Rossi.

Hybrid-electric truck being outfitted with hydrogen-fueled auxiliary power unit, 1997.

Abstract

The use of gaseous hydrogen as an automotive fuel has been a promising goal for some years. Advantages of hydrogen as a fuel for transportation include the following characteristics: When combusted there are no emissions of carbon dioxide, carbon monoxide, or hydrocarbons; it is a renewable fuel source that can be produced easily by several methods (e.g., electrolysis of water using solar energy); and it can be used with fuel cells for highly efficient production of electricity. Hybrid-electric vehicles (HEVs), which combine electric drive systems and internal-combustion engines, also have been an important area of research interest because of their ability to extend the range of electric vehicles with relatively little production of pollutants. The South Coast Air Quality Management District (SCAQMD) has contracted with the College of Engineering-Center for Environmental Research and Technology (CE-CERT) at the University of California, Riverside, to design and develop an HEV that uses a hydrogen-fueled engine as its auxiliary power unit (APU).

One of the significant differences between hydrogen and gasoline is volumetric energy density. Hydrogen stores much less energy per unit of volume than gasoline; therefore, gasoline fuel injectors are inadequate for metering fuel in an engine. This report describes evaluation and development efforts for a hydrogen-fueled internal-combustion engine to be used as an auxiliary power unit in a hybrid-electric vehicle. Four commercially available natural gas injectors (BKM models SP-014, SP-021, SP-051, and SP-010) were evaluated for use with hydrogen. Test results indicate that the sonic flow, pulse-width-modulated electronic gaseous fuel injectors used in this project provided precise, stable and reliable metering of hydrogen gas. This is evident by the linear flow rate curves and also in the low standard deviation error in flow rate during pulse-width-modulation. Plots of flow rate of hydrogen (mg/injection) versus pulse-width (PW) is given for inlet pressures of 25, 50, 75, 100, 125, 150, 175, and 200 psig for the SP-014 and SP-021 injectors. The SP-014 and SP-021 injectors were found to have time delays (time it take the injector to open 50% after the pulse-width signal is sent) of 4.0 ms and 3.0 ms at 200 psig inlet pressure, respectively. These delays times decay linearly to 2.6 ms and 2.3 ms at 25 psig for the SP-014 and SP-021, respectively. It was also found that the time the SP-014 injector is open is 2.0 ms less than the PW signal whereas the SP-021 injector is open 1.4 ms less than the PW signal at a maximum inlet pressure of 200 psig. Based on this analysis, a hydrogen-fueled engine is being implemented as an APU for a hybrid-electric vehicle.

Table of Contents

List of Figures

List of Tables

Acronyms

AC ..... Alternating Current
A/F..... Air-to-Fuel Ratio
APU..... Auxiliary Power Unit
ATDC..... After Top Dead Center
BDC..... Bottom Dead Center
BTDC ..... Before Top Dead Center
CE-CERT ..... College of Engineering, Center for Environmental Research and Technology
CNG ..... Compressed Natural Gas
CO ..... Carbon Monoxide
CVI ..... Constant Volume Injection
DAQ ..... Data Acquisition
DC ..... Direct Current
DMOV ..... Dynamic Minimum Opening Voltage
ECM ..... Engine Control Module
EDIS ..... Electronic Distributorless Ignition System
EGO ..... Exhaust Gas Oxygen sensor
ER ..... Equivalence Ratio
EV..... Electric Vehicle
HC ..... Hydrocarbons
HEV ..... Hybrid Electric Vehicle
HEVT ..... Hybrid Electric Vehicle Testbed
IBE ..... Individual Battery Equalization
ICE ..... Internal Combustion Engine
IMEP ..... Indicated Mean Effective Pressure
kPa ..... kilopascals
MAF ..... Mass Air Flow
mg ..... Milligrams
ms ..... Milliseconds
NAAQS ..... National Ambient Air Quality Standards
NO_x ..... Nitrogen Oxides
Φ ..... Equivalence Ratio or phi
psig ..... Pounds per square inch (gauge)
PW ..... Pulse Width
rpm ..... Revolutions per minute
SCAQMD ..... South Coast Air Quality Management District
SOC ..... State of Charge
STP ..... Standard Temperature and Pressure
UCR..... University of California, Riverside
UCR1 ..... U.C. Riverside's Hydrogen Powered Truck, 1st Generation
V ..... Volt
VRS ..... Variable Reluctance Sensor
WOT ..... Wide Open Throttle
ZEV ..... Zero Emission Vehicle

1.0 Introduction

Despite of impressive improvements in air quality in recent years, the South Coast Air Basin in California still observes air pollutant concentrations significantly above the National Ambient Air Quality Standards (NAAQS). As a result, the health costs attributed to air pollution in Southern California have been estimated to exceed $10 billion per year (Hall et al., 1992, SCAQMD, 1994). Numerous other cities of the world have pollution problems worse than Los Angeles', and over 100 urban areas in the United States have ozone concentrations in excess of the NAAQS. Additionally, concerns about the impact of global climate change as a result of increased concentrations of atmospheric carbon dioxide continue to grow. These issues have led to continued emphasis on the development of low-emitting technologies and cleaner fuels, particularly for motor vehicles.

The Technology Advancement Office the South Coast Air Quality Management District (SCAQMD) has several on-going programs to develop, evaluate, and implement alternative clean burning fuels and technologies. One of the most promising, albeit longer-range, alternative fuels is hydrogen. Among the advantages of hydrogen as a transportation fuel are the following attributes:

- It emits no carbon dioxide, carbon monoxide, or hydrocarbons when burned.
- It is a renewable fuel source that can be produced easily by several methods (e.g., electrolysis of water using solar energy).
- It can be used with fuel cells for highly efficient production of electricity.

While there has been an interest in hydrogen as a fuel for transportation for many years, there are still several technical barriers that need to be overcome before it can become a viable alternative to fossil fuels.

In March, 1992, the College of Engineering-Center for Environmental Research and Technology (CE-CERT) at UC Riverside was funded by the SCAQMD to develop and evaluate a prototype renewable transportation system based on hydrogen. The various aspects of this project addressed the renewable generation of hydrogen from water using solar energy; the development of a hydrogen-vehicle refueling station; and the development and evaluation of a prototype hydrogen-powered vehicle. All phases of the program have been successfully completed (see reports for SCAQMD Contracts 95073/6 and 95073/7). As a result of the evaluation of the prototype hydrogen-powered vehicle (UCR1), it was determined that improvements could be implemented that would improve vehicle drivability, fuel economy, performance, and emissions. Such improvements include increasing the compression ratio and displacement of the engine, using natural aspiration for air induction, using computer-controlled timing advance, and using an electronic fuel injection system for metering the hydrogen to the engine.

CE-CERT has since been contracted to complete two phased of a three phase project to address these issues In Phase I, the design/specification of the engine, fuel injection system, computer control module, and the instrumentation and data acquisition system was conducted. The results of this phase of the project are given in the Final Report "Development and Evaluation of a

Hydrogen Fuel Power Plant for a Hybrid Electric Vehicle" which was submitted to the SCAQMD. Phase II consisted of the seven tasks listed below:

Task 1: Test Bench Fabrication
Task 2: Hydrogen Fuel Injection System
Task 3: Ignition System
Task 4: Engine Control System
Task 5: Fuel Injector, ignition System, and ECM Bench Test
Task 6: HEV Battery Balance Control System
Task 7: HEV Overall Energy Management Strategies

The results of these tasks are discussed in this report.

2.0 Background

The development of alternatives to the petroleum-fueled internal combustion engine (ICE) for personal transportation offers significant opportunities both to decrease the dependence of the U.S. on imported fuels and to decrease the adverse environmental effects of petroleum.

Electric vehicles (EVs) offer an attractive alternative to internal combustion powered vehicles due to the potential for the decreased cost to purchase, operate, and maintain an electric drivetrain relative to an ICE. EVs are classified as Zero Emission Vehicles (ZEVs). Even when the ultimate source of their energy (i.e., the electric utility) is considered, EVs offer credible solutions to both the energy dependence and vehicle emission problems—especially in California.

The main drawback of EVs is their limited range, due to the low energy density of current electric energy storage devices (i.e., batteries, ultracapacitors, flywheels) relative to that of petroleum. Hybrid Electric Vehicles (HEVs) on the other hand, offer a means to attain the low emissions benefits of EVs and the performance characteristics that consumers have come to expect due to their experience with ICEs. The extent to which the energy dependence problem is solved will depend on the fuel used by the Auxiliary Power Unit (APU) and the efficiency of the total HEV energy conversion process.

Tasks 1-5 of this contract focused on the specification and development of the technologies required for the production of a Hydrogen Fuel Power Plant for a Hybrid Electric Vehicle. Tasks 6 and 7 focused on the solution to two open HEV research problems. These problems are identified and discussed in the following two sections.

2.1 Hydrogen Combustion

Hydrogen has been considered as a fuel for internal combustion engines for more than 100 years. In 1820, Cecil was the first to recommend the use of hydrogen as a fuel for powering engines (Cecil, 1822). Published reports on hydrogen as a fuel continued into the first half of the 20th Century. In particular, just prior to and during World War II, interest in hydrogen increased. For example, in the 1930s, Rudolf Erren converted over 1000 vehicles to run on hydrogen or hydrogen/gasoline blends (Hoffman, 1981). In the 1940s, Oehmichen reported efficiencies of over 50% from an engine running solely on hydrogen (Oehmichen, 1942).

Although interest in hydrogen fuel waned immediately following the end of World War II, some research into hydrogen vehicles continued, most notably that of R.O. King in Canada (King et al., 1955, 1956). In the 1970s, primarily as a result of the oil crisis, there was a resurgence of research into the possibility of hydrogen-fueled transportation with programs initiated in Japan, West Germany, and the United States. In the last 15 years, research on hydrogen has been reported by Mazda, BMW, and Mercedes Benz, and several university researchers (Swain et al., 1983, Koyanagi et al., 1994). A detailed review of research on hydrogen as a fuel for surface transportation is provided in Norbeck, et al. (1996).

Hydrogen has several unique properties, some quite different from conventional liquid fuels, which are summarized in Table 2-1 (Norbeck et al., 1996).

Table 2-1. Hydrogen's properties as a transportation fuel.

Characteristic	Properties
Limits of flammability	Hydrogen has a wide range of flammability in comparison with other fuels. Hydrogen engines, therefore, can be operated more effectively on excessively lean mixtures than gasoline engines. As little as 4% hydrogen by volume with air produces a combustible mixture.
Minimum ignition energy	For hydrogen, the minimum ignition energy is about an order of magnitude less than that required for gasoline. This enables lean mixtures and prompt ignition. However, hydrogen also can be ignited by hot spots on the cylinder.
Quenching gap or distance	The combustion flame typically travels closer to the cylinder wall than a gasoline flame. This can increase the tendency for backfire since the flame can more readily get past a nearly closed intake valve.
Self-ignition temperature	The self-ignition temperature is relatively high. This allows larger compression ratios to be used in a hydrogen engine.
Flame speed	The flame speed is nearly an order of magnitude higher than that of gasoline. For stoichiometric mixtures, hydrogen engines can approach the thermodynamically ideal engine cycle. For leaner mixtures, however, flame velocity decreases significantly.
Diffusivity	Hydrogen's ability to disperse in air is considerably greater than gasoline's.
Density	Hydrogen has extremely low density, meaning very large volumes are necessary for storage and combustion.

The UCR1 truck uses the Constant Volume Induction (CVI) system for metering the hydrogen to the engine (Lynch, 1983). Several difficulties with the CVI system, most notably the additional flow of a small amount of oil (needed for cam and valve lubrication) results in pre-ignition.

Electronic fuel injection technology, using solenoid actuated injectors feeding fuel into the throttle body or into the intake manifold near the intake valve, has been developed over the past three decades in response to air pollution requirements. The electronic system, using engine sensors and microprocessor control, allows precise fuel metering and cylinder distribution, cold start enrichment closely controlled to the temperature of the engine and air, deceleration and overspeed cutoff, and protection from driver abuses such as flooding. This technology was introduced for gasoline powered engines first by Volkswagen and Bosch in 1967 and became commonplace in the following decade.

Oehmichen (1942) reported extensive measurements taken using a mechanically implemented sidewall injection of hydrogen. These data, collected over 60 years ago, remains among the most instructive. The injection scheme, however, is not appropriate for a modern engine.

MacCarley and Van Vorst (1980) implemented electronically controlled hydrogen injection to a dynamometer mounted Yamaha TX-650 test engine. Their research showed that the conventional gasoline injectors were much too small for the required hydrogen flow. They designed, fabricated and tested several prototype injectors. By use of a capacitor discharge driver for the coil they were able to achieve very fast opening and closing, as low as 1 ms. The most advanced injector was able to inject 240 cc hydrogen at 30 psig (41 mg) in a 5 ms pulse.

Varde and Frame (1984, 1985) developed a fuel injection system similar to MacCarley and Van Vorst. Later, they developed a hydraulically driven injector. Flow rates are not given for the electronic injector but they are well below those of MacCarley's for the hydraulic injector. Both the injectors appear to be slower than those of MacCarley, as the data reported is taken at engine speeds at or below 2100 rpm.

Homan et al. (1983) studied the combustion of hydrogen injected late in the compression stroke and ignited just after the beginning of injection. A hydraulically driven injector was used and data is presented at engine speeds up to 1500 rpm. This paper is primarily of interest for its NO_x, indicated mean effective pressure (IMEP) and indicated thermal efficiency data.

Krepec and students developed an injector designed to operate for a 3 ms injection period with hydrogen inlet pressure of 200 bars - well above that thought practical for the present system (Giannacopoulos et al., 1986).

Glasson and Green (1994) have designed injectors for injection of hydrogen at high pressure (80 bar).

The 20 year old work of MacCarley and Van Vorst is the most instructive with regard to injector design and implementation. Their injectors have the highest flow rates and are among the fastest operating, but unfortunately their work has not been implemented commercially.

Although electromagnetic gasoline injectors are commonly available, they cannot be used for gaseous fuel injection due to the much larger volumes of fuel that must be injected as compared to the liquid form. Specially developed injectors are available to flow 100 g/s of natural gas (Barkhimer et al., 1995). These commercially available natural gas injectors will be used as the baseline design for the hydrogen injectors.

2.2 Battery Balance

Maintenance of a balanced battery pack is a difficult problem in existing electric vehicles. Due to minor differences in battery energy capacities, the repeated discharge/charge cycle will result in the various batteries in the pack having diverse state of charges (SOC). Severely unbalanced battery packs can result in permanent battery damage. Since manufacturer battery specifications refer to a single battery, while vehicle applications involve numerous batteries in series strings, divergence of the SOC's of the individual batteries is believed to be one of the reasons for the discrepancy between manufacturer battery life cycle specifications and the actual life cycle experienced onboard vehicles (Dickinson and Swan, undated).

Currently, balance of the battery pack is typically accomplished by controlled over-charging. Ideally, over-charging refers to holding each individual battery terminal voltage at a specified

value (e.g., V_f = 14.5 V) for an extended duration. However, since batteries onboard a vehicle are charged as a series string, the ideal situation is rarely achieved. Instead, the terminal voltage of a series string of N batteries is held at $N*V_f$ for the specified amount of time. In this scenario, some batteries are overcharged, resulting in gassing which further decreases their charge capacity. Other batteries are undercharged, possibly leading to permanent battery damage during discharge based on the estimated SOC of the battery pack. In HEVs, the battery balance problem is expected to be greater due to more frequent SOC cycling of the batteries.

In Task 6 of this project, CE-CERT has investigated automatic electronic methods for controlling the per battery charging process to maintain battery balance. Such a system would alleviate EV and HEV owners of a maintenance task that must currently be completed monthly in a manual fashion.

2.3 Energy Management

HEVs employ alternative power sources (i.e., batteries or H_2 ICE) for meeting drivetrain power requirements. An HEV's energy management strategy determines how power in a hybrid powertrain should be produced and distributed as a function of various vehicle parameters (e.g., power demand, battery SOC, APU power level, etc.). Characteristics of each major HEV component will provide the limits within which the strategy will operate. The objective is that the energy management strategy optimizes the HEV operation in terms of overall energy efficiency, emissions, and secondary issues such as noise. Research at CE-CERT under Task 7 is developing simulation models of the HEV components for energy management simulation, and a theory for the design of optimal energy management strategies.

3.0 Hydrogen Combustion Theory

The requirement for the fuel injectors are based on two engine configurations. The first is a variable speed engine for a conventional vehicle with the following specifications:

1. Eight cylinders, natural aspirated
2. Approximate displacement of 350 cu. in. (5.7 liters)
3. Maximum engine speed of 5,000 rpm.

The second engine is a constant speed engine for a hybrid electric vehicle with the following specifications.

1. Four cylinders, naturally aspirated
2. Approximate displacement of 36 cu. in. (2.2 liters)
3. Maximum engine speed of 3,500 rpm

Because the injector requirements for the variable speed engine are more stringent, in terms of fuel flow rate and injection time, than for the constant speed engine, the design of the injectors will be base on these requirements. The appropriate design calculations are given below.

3.1 Fundamental Equation for the Combustion Hydrogen and Air

$2H_2 + O_2 = 2H_2O$

Number of moles of H_2 for complete combustion = 2 moles

Number of moles of O_2 for complete combustion = 1 mole

Number of moles of N_2 in air = # of moles of O_2 x (79% N_2 in air/21% O_2 in air)
= 1 mole of O_2 x (79% N_2 in air/21% O_2 in air)
= 3.762 moles N_2

Number of moles of air = moles of O_2 + moles of N_2
= 1 + 3.762
= 4.762 moles of air

Weight of O_2 = 1 mole of O_2 x 32 g/mole
= 32 g

Weight of N_2 = 3.762 moles of N_2 x 28 g/mole
= 105.33 g

Weight of air = weight of O_2 + weight of N_2 (1)
= 32g + 105.33 g
= 137.33 g

Weight of H_2 = 2 moles of H_2 x 2 g/mole
= 4 g

Stoichiometric Air/Fuel (A/F) ratio for H_2 and air:

Based on mass:
A/F = mass of air/mass of fuel = 137.33 g/4 g = 34.33:1

Based on volume:
A/F = volume (moles) of air/volume (moles) of fuel = 4.762/2 = 2.381:1

Percent of combustion chamber occupied by H_2 for a stoichiometric mixture:

$$\% H_2 = \text{volume (moles) of } H_2/\text{total volume} \quad (2)$$
$$= \text{volume (moles) of } H_2/(\text{volume (moles) of air} + \text{volume (moles) of } H_2)$$
$$= 2/(4.762 + 2)$$
$$= 29.57\%$$

3.1.1 Maximum Injector Pulse Width for the Variable Speed Engine

Using 5,000 rpm as the top engine speed for the variable-speed engine, the crankshaft will complete one revolution in 12 ms (1 min/5000 rev x 60 s/min). Of the 360° of crank rotation during one revolution, 145° is used for hydrogen induction. This leaves only 4.83 ms (12 ms x 145°/360°) available for hydrogen induction at maximum engine speed.

3.1.2 Maximum Hydrogen Flow Rate for the Constant Speed Engine

Using 3,500 rpm as the top engine speed for the constant speed engine, the crankshaft will complete one revolution in 17 ms (1 min/3500 rev x 60 s/min). Of the 360° of crank rotation during one revolution, 145° is used for hydrogen induction. This leaves only 6.90 ms (17 ms x 145°/360°) available for hydrogen induction at maximum engine speed.

3.2 Hydrogen Flow Rate Calculations

From equation (2) in Section 3.1, an engine operating at a stoichiometric mixture of hydrogen and air, the hydrogen will occupy approximately 30% of the combustion chamber. For an engine operating on hydrogen fuel, however, it is preferred to operate the engine with a very lean (excess air) A/F ratio to reduce the combustion chamber temperature and thus the amount of NO_x formation. Operating with a lean A/F ratio will result in less hydrogen being injected into the engine, which in turn corresponds to the hydrogen occupying less of the combustion chamber.

For the purpose of this report, the degree of air-to-fuel leanness will be expressed using equivalence ratio (ER) or phi (Φ). ER (Φ) is equal to the stoichiometric A/F ratio divided by the actual A/F ratio. For a stoichiometric mixture, the actual A/F ratio is equal to the stoichiometric A/F ratio and thus the ER (Φ) equals one. For lean A/F ratios, ER (Φ) will be a value less one.

For example, an ER (Φ) of 0.5 means that there is only enough fuel available in the mixture to oxidize with half of the air available. Another way of saying this is that there is twice as much air available for combustion than is theoretically required. The importance of operating the engine at low ER (Φ) is illustrated in **Figure 1**. One can see that there is a substantial difference in NO_x formation when operating an engine at an ER (Φ) of 0.6 compared to operating it at an ER (Φ) of 0.4.

For an engine operating at an ER (Φ) of 0.4 (the design target for this project), the 30% of hydrogen in the combustion chamber for a stoichiometric mixture will decrease to approximately 14%. This value is calculated below:

$$ER\ (\Phi) = (A/F_{stoich})/(A/F_{actual})$$

or

$$A/F_{actual} = (A/F_{stoich})/(\Phi)$$
$$= 34.33/0.4$$
$$= 85.825$$

By definition, A/F_{actual} = Wt of air/Wt of fuel

From equation (1) in Section 3.1, the weight of air was found to be equal to 137.3 g.

Therefore:

$$A/F_{actual} = 137.3\ g/(X \text{ moles of } H_2 \times 2\ g/mole)$$
$$= 137.3/(2X \text{ moles of } H_2)$$
$$= 85.825$$

Solving for X:

$$2X \text{ moles of } H_2 = 137.3/85.825$$
$$X \text{ moles of } H_2 = 1.60/2$$
$$X = 0.8 \text{ moles of } H_2$$

Percent of combustion chamber occupied by hydrogen for an ER (Φ) = 0.4

$$\% = \text{Volume of } H_2/\text{Total volume}$$
$$= \text{Volume of } H_2/(\text{volume of air} + \text{volume of } H_2)$$
$$= 0.8 \text{ moles of } H_2/(4.762 \text{ moles of air} + 0.8 \text{ moles of } H_2)$$
$$= 0.8/5.562$$
$$= 14\%$$

Figure 3-1. Plot of NOx output vs. equivalence ratio (Φ) (Das, 1990)

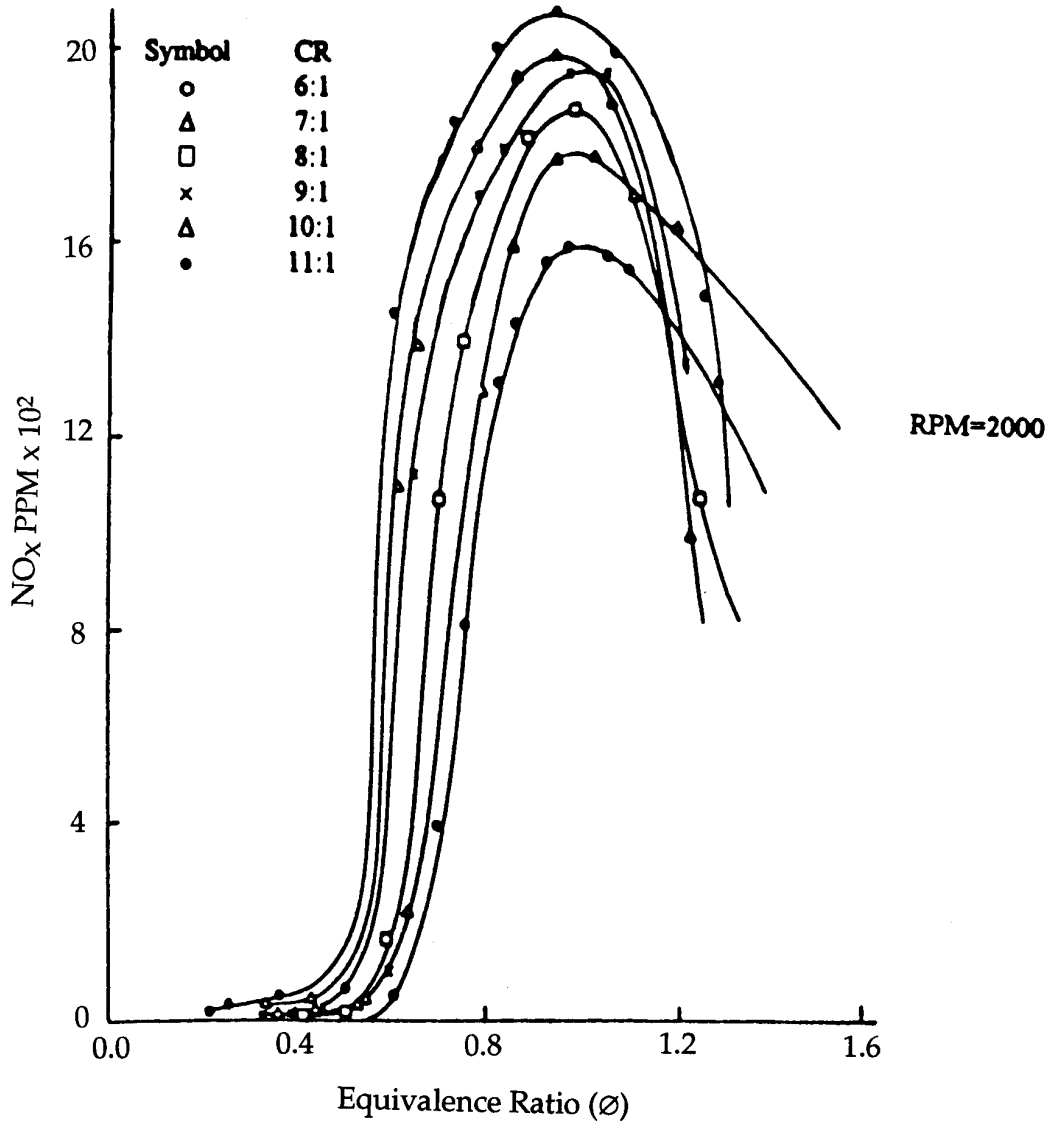

3.2.1 Maximum Hydrogen Flow for the Variable Speed Engine

Calculations for the maximum hydrogen flow rate for the variable speed engine are based on a cylinder size of 44 cu. in. This cylinder size corresponds to an 8 cylinder engine with a displacement of approximately 350 cu. in. (5.7 liters).

Using this cylinder displacement, the mass of hydrogen required for each intake stroke can be calculated as follows:

Mass of H_2 = Combustion chamber volume x % H_2 x density of H_2 at STP
= 44 cu. in. x 14% x (.0.00523 lb./cu. ft x 1 cu. ft/1728 cu. in.)
= 0.000018538 lb.
= 8.4 mg

Note: The mass of H_2 calculated is based on an engine with a 100% volumetric efficiency. Actual mass would be somewhat less than this amount.

Using the 4.83 ms PW calculated in Section 3.2.1 and dividing this value into the 8.4 mg of hydrogen calculated above, the injector needs to flow 1.74 mg of H_2/ms at the maximum engine speed.

3.2.2 Maximum Hydrogen Flow for the Constant Speed Engine

Calculations for the maximum hydrogen flow rate for the constant speed engine are based on a cylinder size of 136 cu. in. This cylinder size corresponds to a 4 cylinder engine with a displacement of approximately 144 cu. in. (2.2 liters).

Using this cylinder displacement, the mass of hydrogen required for each intake stroke can be calculated as follows:

Mass of H_2 = Combustion chamber volume x % H_2 x density of H_2 at STP
= 36 cu. in. x 14% x (.0.00523 lb./cu. ft x 1 cu. ft/1728 cu. in.)
= 0.00001525 lb.
= 6.9 mg

Note: The mass of H_2 calculated is based on an engine with a 100% volumetric efficiency. Actual mass would be somewhat less than this amount.

Using the 6.90 ms PW calculated in Section 3.2.2 and dividing this value into the 6.9 mg of hydrogen calculated above, the injector needs to flow 1.0 mg of H_2/ms at the maximum engine speed.

4.0 Approach

4.1 Hydrogen Test Set-Up

A layout of the Injector and Engine Control Module (ECM) Test Bench is shown in **Figure 4-1**. The test bench has two hydrogen flow meters plumbed in series. One of the meters is manufactured by Porter and the other by Micromotion. The Porter meter will be used to measure flows under 35 standard cubic feet per minute (scfm). For flows between 35 and 150 scfm, the Micromotion will be used. The accuracy of the Porter and Micromotion meters are 0.5 % and 0.1% of full scale, respectively.

Figure 4-1. Layout of test bench

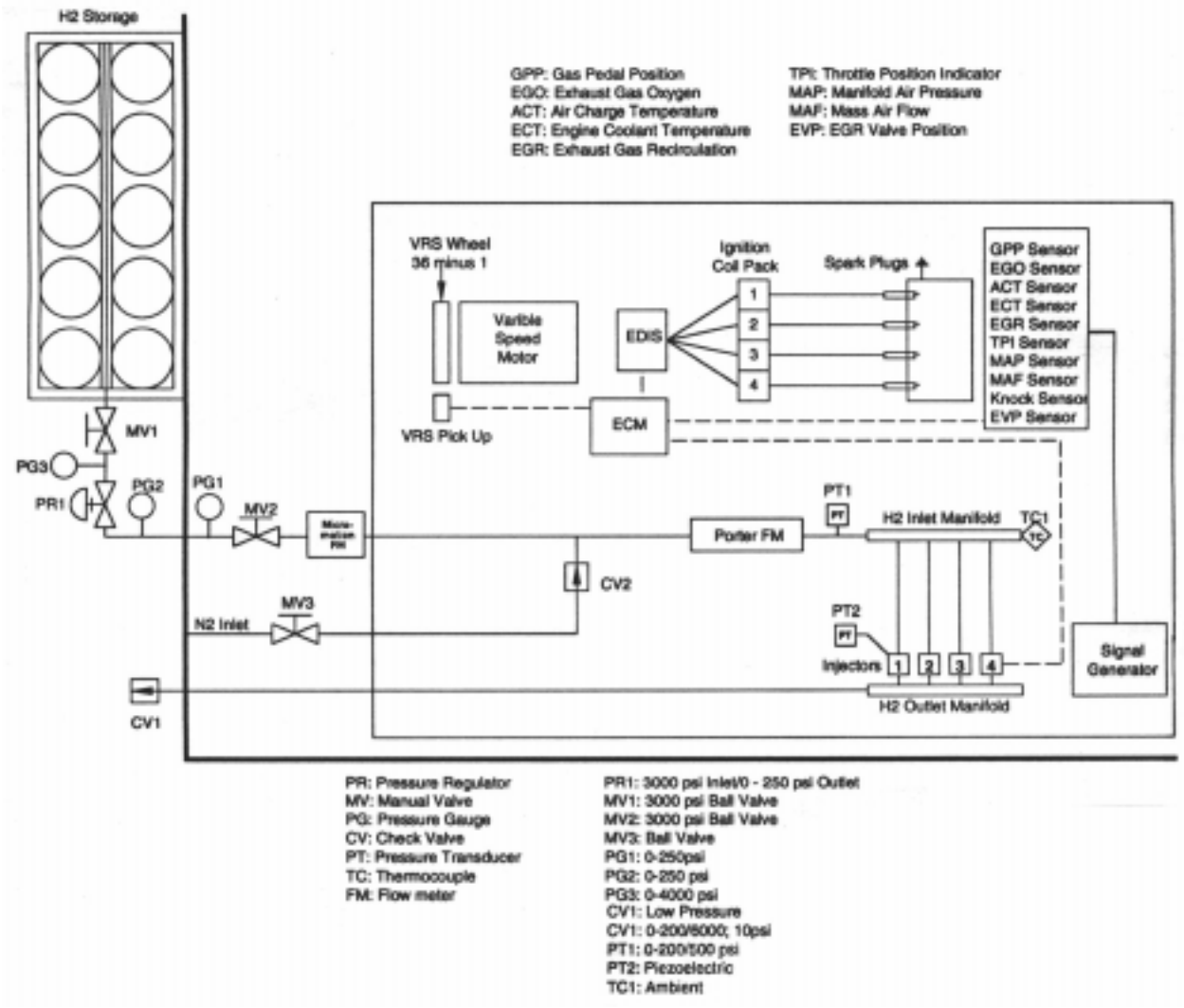

Hydrogen from the hydrogen storage system is regulated to the test pressure at pressure regulator 1 (PR1) prior to entering the flow meters. From the flow meters, the hydrogen enters the H_2 inlet manifold where the pressure and temperature of the hydrogen is measured and recorded. The inlet manifold distributes the hydrogen to four injectors which are installed in the H_2 outlet manifold. The hydrogen is exhausted outside the building via a vent stack. A PCB piezoelectric pressure transducer Model 112A is installed in the #1 manifold block to measure the outlet pressure of the injector. The PCB has a range of 0 to 10,000 psi.

To operate these injectors independently of the ECM, four driver circuits were developed and incorporated into a test circuit as shown in **Figure 4-2**. This circuit is capable of firing one to four injectors in order to characterize hydrogen flow under a range of possible engine operating conditions. The input signal to the injector drive circuitry is provided by a function generator and pulse-width modulator as shown in **Figure 4-3**. The signal generator is a Tektronix CFG280 11 MHz function generator and is used to control the time between injector firing. The pulse-width modulator is used to control the time that the injector is energized. A schematic of the pulse-width modulator circuit is shown in **Figure 4-4**. This modulator can control pulse-widths from 5 to 95% duty cycle (duty cycle is the time the injector is open relative to the total time. For example, a 40% duty cycle and a pulse width (PW) of 4 ms means that the injector will be open for 4 ms and closed for 6 ms for a total cycle of 10 ms (PW = total cycle time x duty cycle). By using the modulator in conjunction with a signal generator, frequency and duty cycle can be controlled within the entire range of the test matrix. Injector firing and pulse-width duration is displayed on a Tektronix 5112 Dual Beam Oscilloscope. The modulator and signal generator were used to fire the injectors while the Motec engine control module was being developed.

Figure 4-2. Test circuit

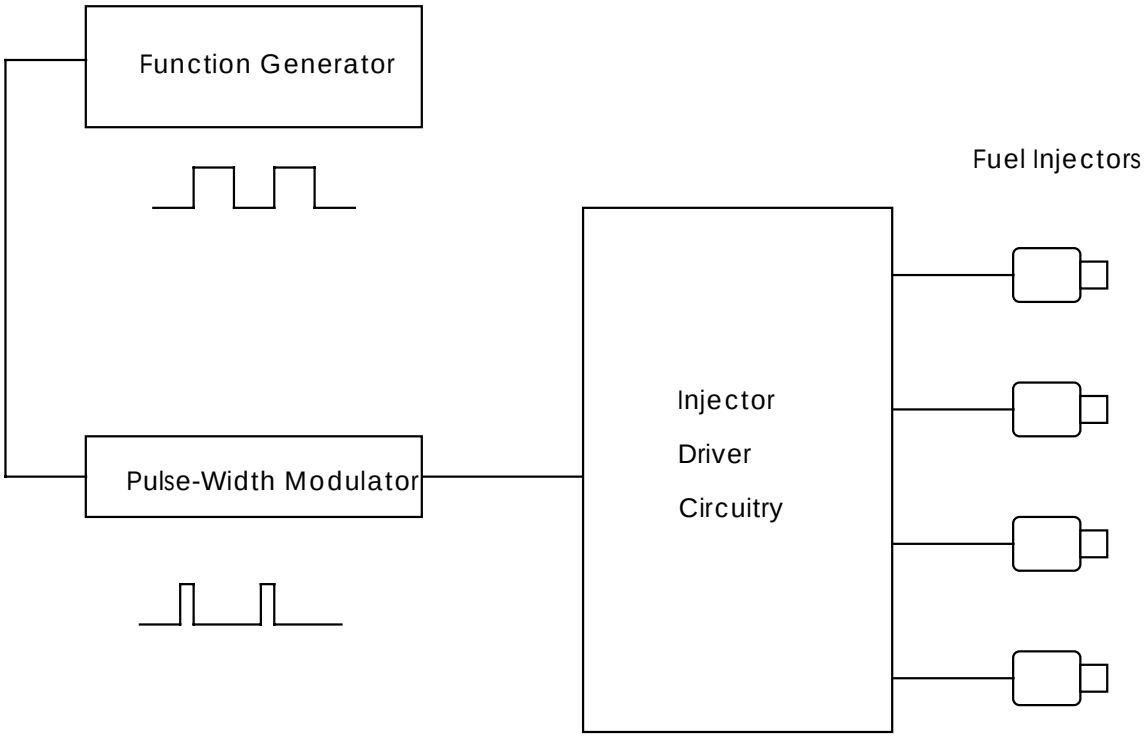

Figure 4-3. Injector driver circuit

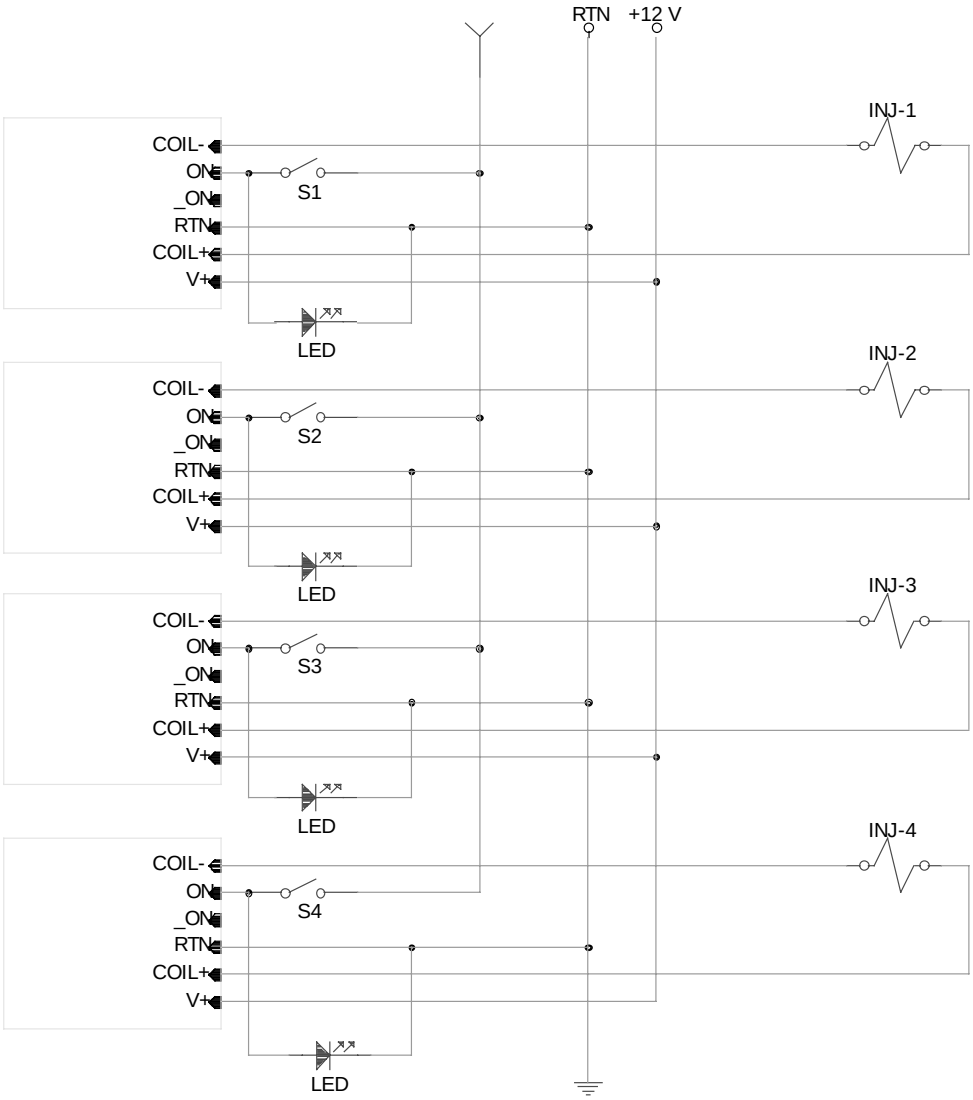

To simulate the speed of the engine, an Astro Cobalt-40 Sport Motor #640 variable speed motor was selected to drive the 36 minus one tooth Variable Reluctance Sensor (VRS) wheel. The VRS provides timing information to the ECM every 10° of crankshaft rotation.

The ignition system consists of an Electronic Distributorless Ignition System (EDIS) module, coil packs, and four spark plugs and spark plug wires.

Figure 4-4. Schematic of the pulse-width modulator circuit

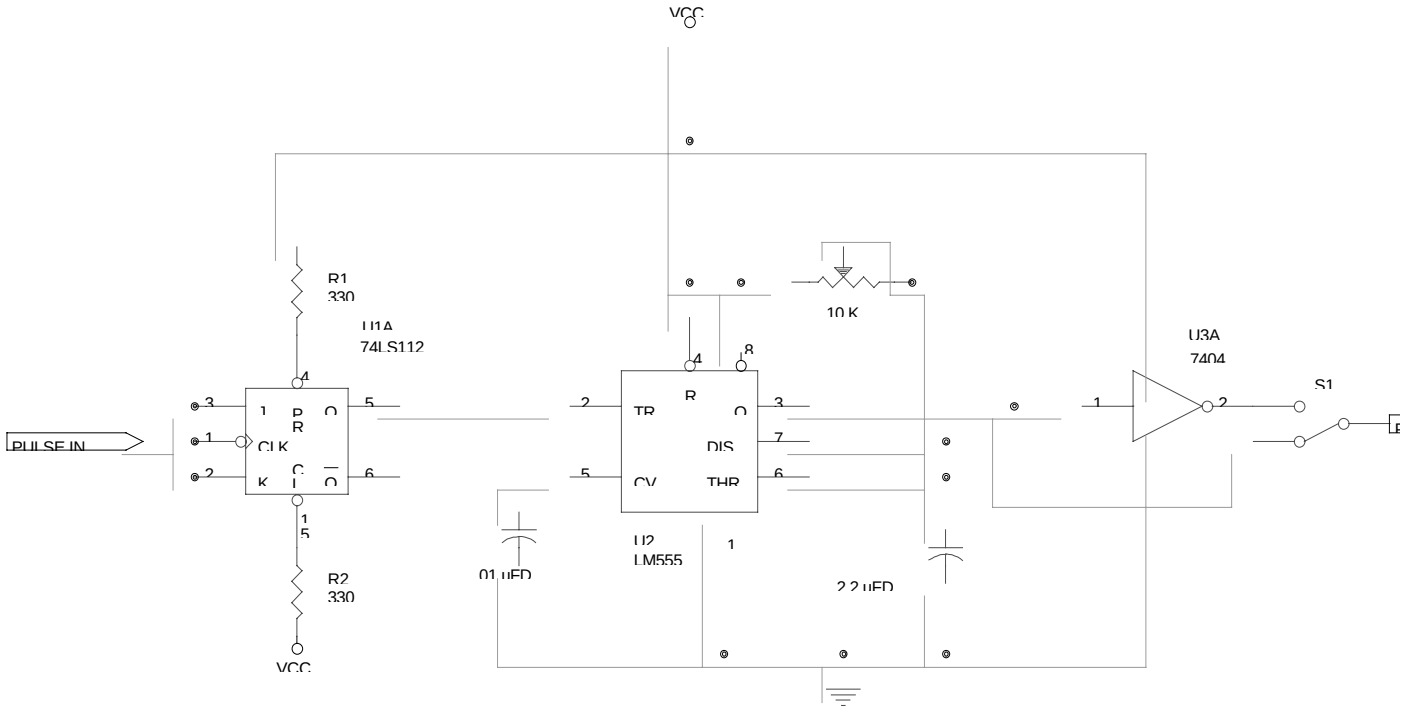

4.2. Fuel Injectors

Four Servojet pulse-width-modulated electronic natural gas injectors, models SP-010, SP-014, SP-021, and SP-051 manufactured by BKM were selected to be evaluated for use with hydrogen (Figure 4-5).

Figure 4-5. BKM SP-051 injectors with 12-inch ruler for scale

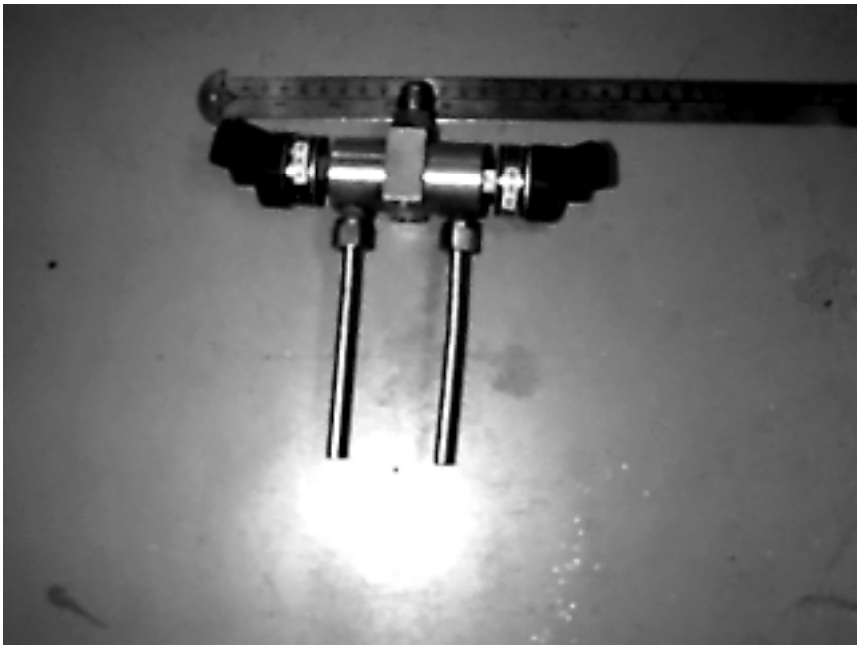

4.2.1. Injector Description

The Servojet pulse-width-modulated electronic gas injector is a two way, normally closed, solenoid operated valve. Designed with corrosion resistant materials, it meters gaseous fuels into the intake system of internal combustion engines. The injector is a cartridge design for easy installation. These injectors are typically pulse-width-modulated to meter fuel quantity at any operating frequency, even above 100 Hz. With sonic flow across the valve inlet when fully open, mass flow is approximately proportional to the supply pressure (Barkhimer et al., 1995).

4.2.2 Injector Basic Design and Function

The basic design of the gas injector was derived from the fast responding solenoid valve which is described in detail by Barkhimer et al. (1983). The injectors are composed of a solenoid coil and valve assembly. The coil assembly consists of solenoid winding and electrical connection. The valve assembly is comprised of the valve body which holds the solenoid armature, ball poppet and seat. **Figure 4-6** shows the operating concept of the injector. The cross-section of the actual injector is shown in **Figure 4-7.** With the solenoid de-energized, the supply pressure, assisted by a spring, forces the solenoid ball poppet on its seat, prohibiting gas flow. When the solenoid is energized, the ball poppet is lifted off the seat and held against the stop. Gas then passes through the valve seat and outlet port of the injector. The solenoid is a low resistance coil designed for rapid response, and is typically actuated by a current to 4 amperes, then reduced and held at 1 ampere to conserve energy for the duration of the energized time (pulse-width) (Barkhimer et al., 1995).

Figure 4-6. Operating concept of the hydrogen injector (Barkhimer et al., 1995)

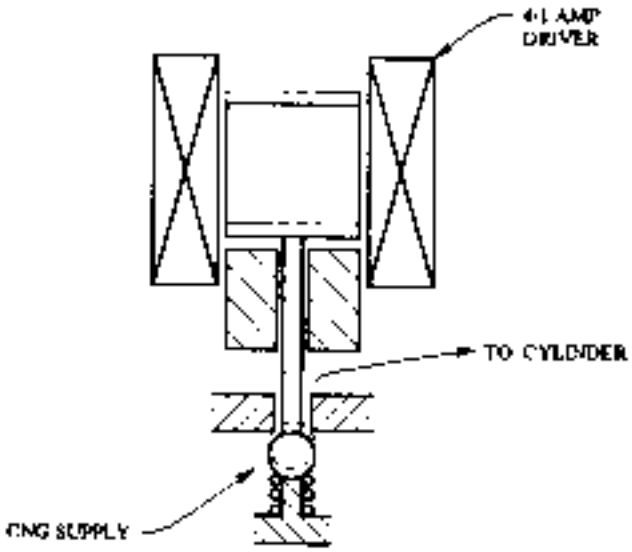

Figure 4-7. Injector cross-section (Barkhimer et al., 1995)

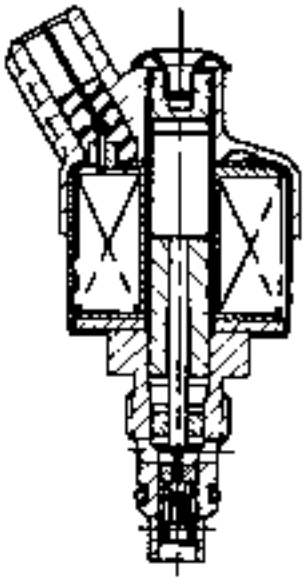

4.2.3. Injector Gas Flow Characteristics

In electronically controlled fuel-injection systems, solenoid operated injectors are used for fuel metering. Gaseous fueling consistency between injectors and cycles is just as important as with liquid injectors. The static gaseous flow rate is defined by the following formula:

$$Q_{static} = C_d \cdot A \cdot V_t ,$$

where C_d = Coefficient of discharge
A = Area of throat at valve seat
V_t = Velocity at throat

For sonic flow, the velocity of gas through the orifice is given by:

$$V_t = \sqrt{\frac{\gamma \cdot P_t}{\rho_t}} ,$$

where γ = Ratio of specific heats
P_t = Pressure at throat
ρ_t = Density at throat

The static mass flow rate becomes:

$$Q_{static} = \frac{KAP_1}{\sqrt{T_1}} ,$$

where P_1 = Absolute inlet pressure
T_1 = Absolute inlet temperature
K = Constant

provided that,

$$\frac{P_2}{P_1} \leq r ,$$

where P_2 = Absolute outlet pressure
r = Critical pressure ratio (0.546 for methane and 0.528 for hydrogen)

and,

$$r = \left(\frac{2}{\gamma + 1} \right)^{\frac{\gamma}{\gamma - 1}}$$

Therefore, it is recommended the ratio of manifold absolute pressure to absolute supply pressure not exceed the critical pressure ratio to maintain the sonic flow characteristic. The metering capability of these four injectors, using natural gas, are shown in **Figures 4-8, 4-9, 4-10,** and **4-11**. These data were obtained from the manufacturer, BKM.

Figure 4-8. Natural gas metering capability of the SP-014 injector (BKM, 1996)

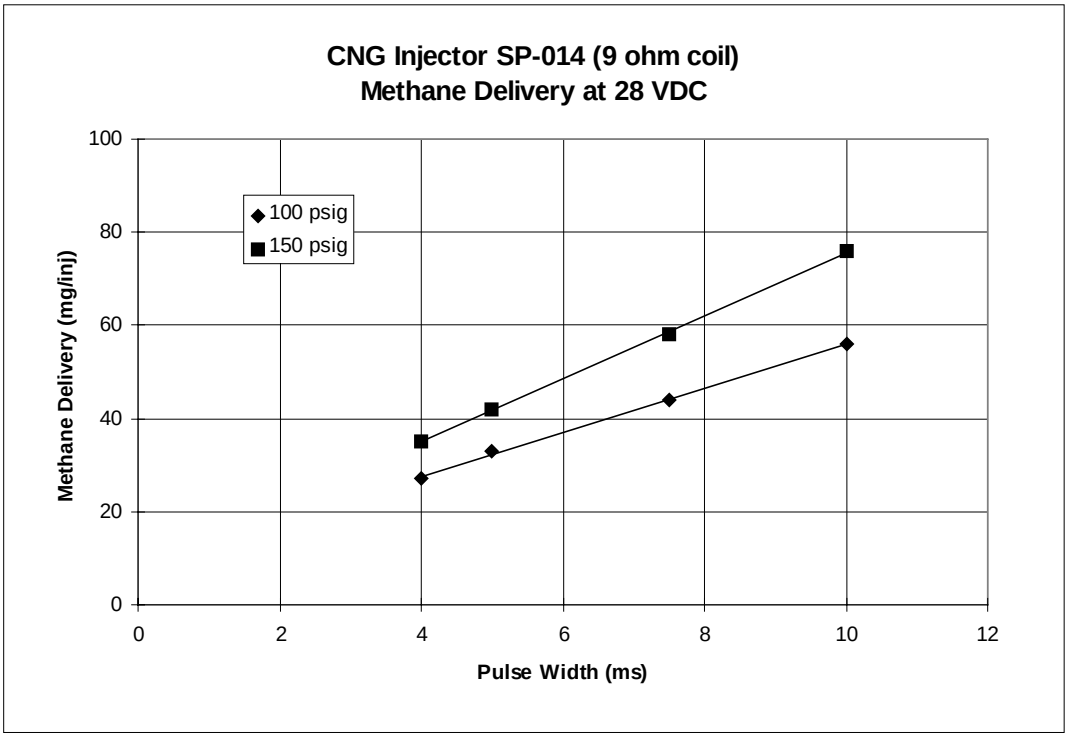

Figure 4-9. Natural gas metering capability of the SP-021 injector (BKM, 1996)

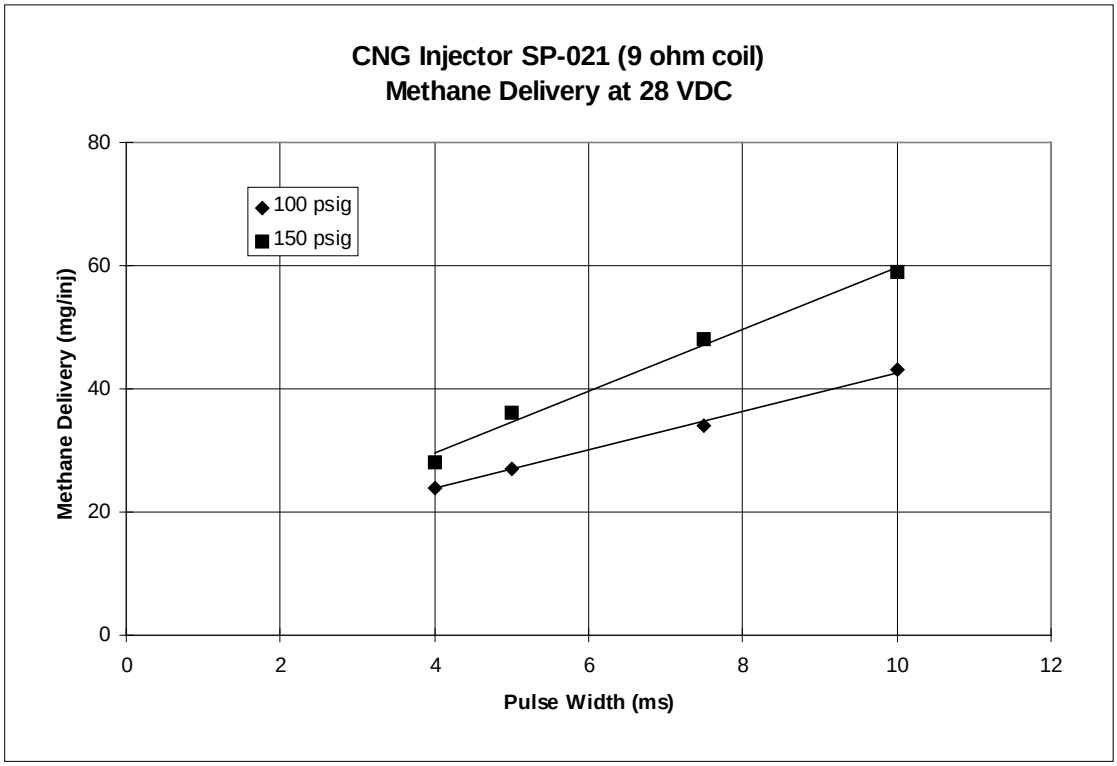

Figure 4-10. Natural gas metering capability of the SP-051 injector (BKM, 1996)

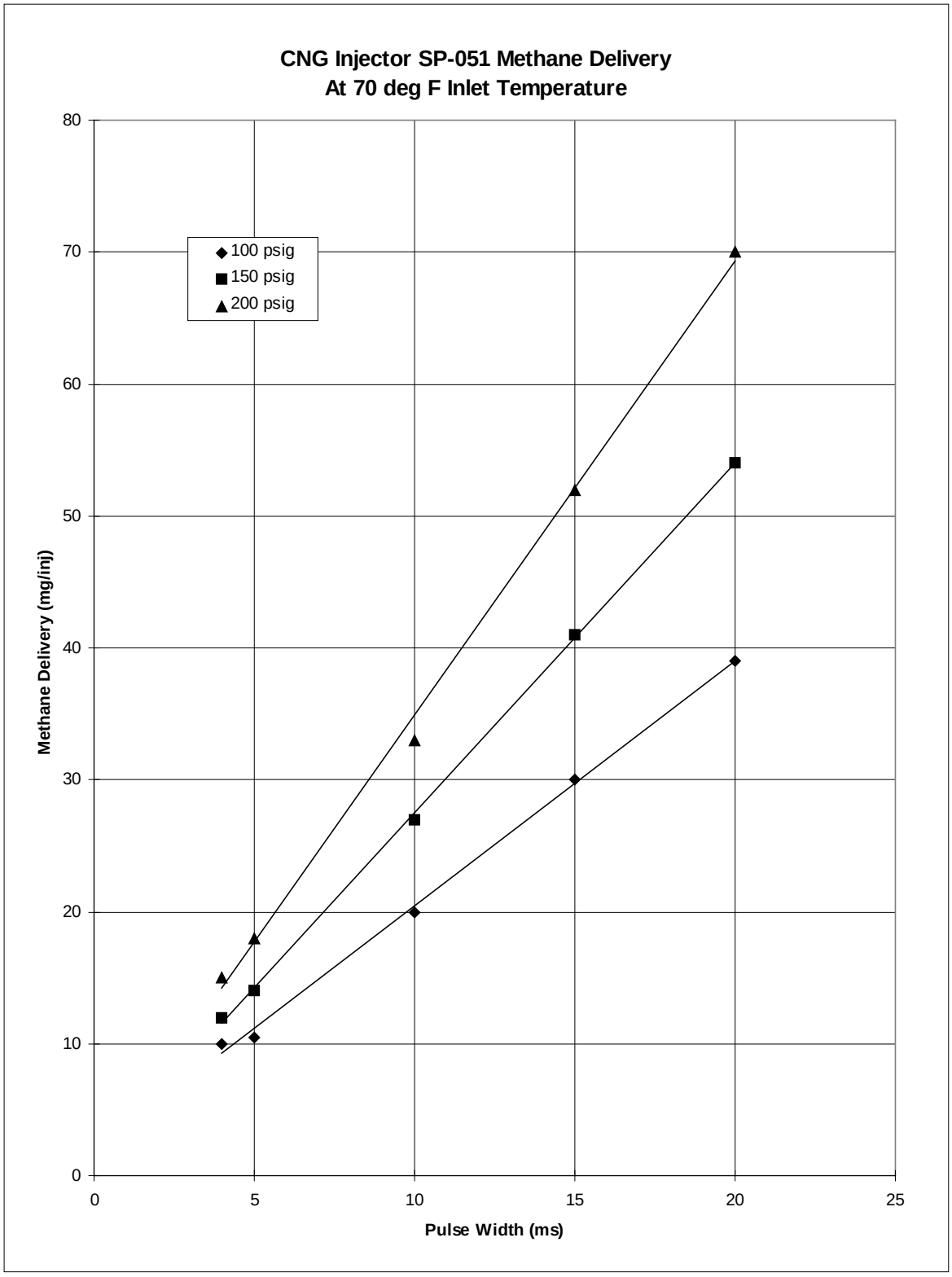

Figure 4-11. Natural gas metering capability of the SP-010 injector (BKM, 1996)

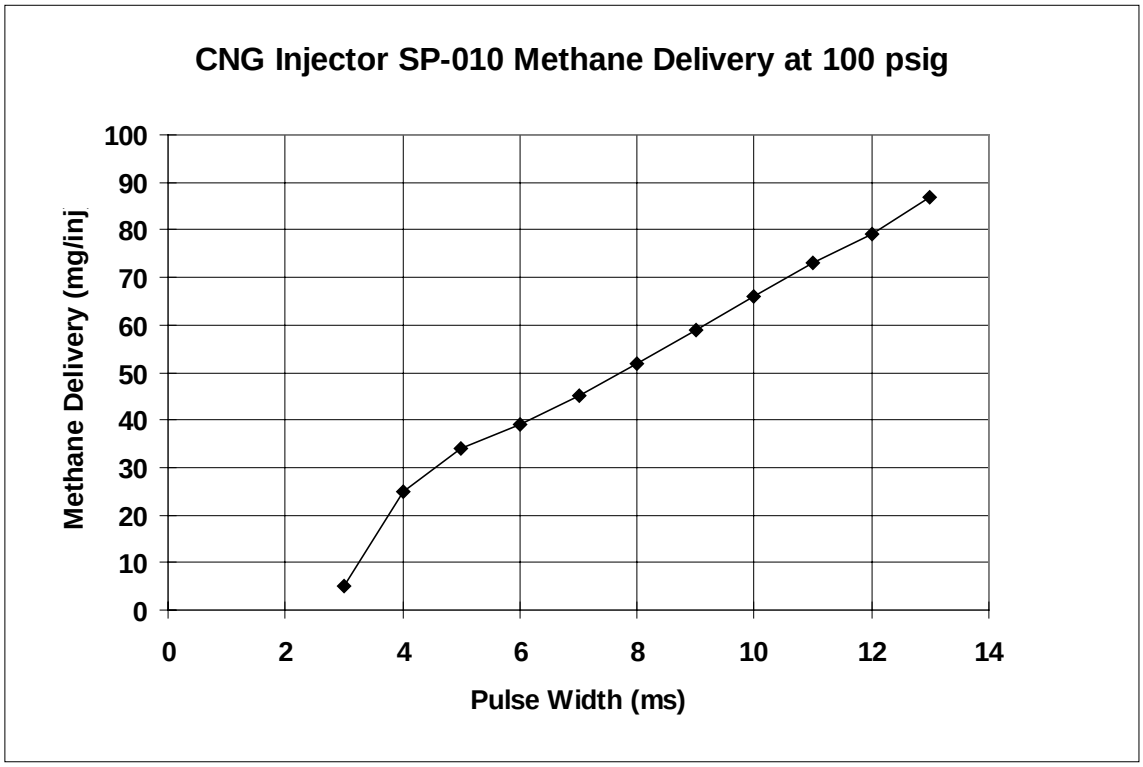

4.2.4. Effect of Voltage Variation

Under certain circumstances, such as starting and low battery operation, normal voltage is not available. Having a low resistance coil winding, the minimum opening voltage of the Servojet gas injector is less than 4 Volts DC. The minimum current required to actuate the injector from the closed to open position is approximately 2.5 amperes at 690 kPa (100 psig) inlet pressure. Due to the low resistance coil and the current limiting driver circuit characteristics, the injector is not as sensitive to low battery voltage as are the high resistance units. Furthermore, the required flow rate of injectors at low voltage is to provide a satisfactory start, after which full battery charging voltage is normally available.

Experiments have shown the dynamic minimum opening voltage (DMOV) at 690 kPa (100 psig) supply pressure is below 4.5 Volts DC for model SP-021 injectors. The DMOV is defined as the voltage at which the flow rate at 10 ms pulse width exceeds 50% of the flow at 14.0 VDC. **Figure 4-12** shows the deviation of injected CNG quantity at 690 kPa (100 psig) supply pressure and various pulse widths over a supply voltage range of 4.0 to 14.0 Volts DC (Barkhimer et al., 1995).

4.3 Fuel Injector Leakage

Leakage rates for the four BKM injector models were determined to evaluate the possibility of pre-ignition due to hydrogen leakage past the injectors into the engine block. The four injector

models were tested at pressures of 50, 100, 150, and 200 psig. Pressurized hydrogen gas from the K-bottle rack was piped to the injector assembly. At the outlet port of the injector assembly a plastic tube was attached. This plastic tube was then connected to a Humonics Optiflow 520 Digital Flowmeter. The hydrogen leakage flow rate in cc/min was recorded at 30-second intervals for a total of 30 minutes.

Figure 4-12. Effect of supply voltage (BKM, 1996)

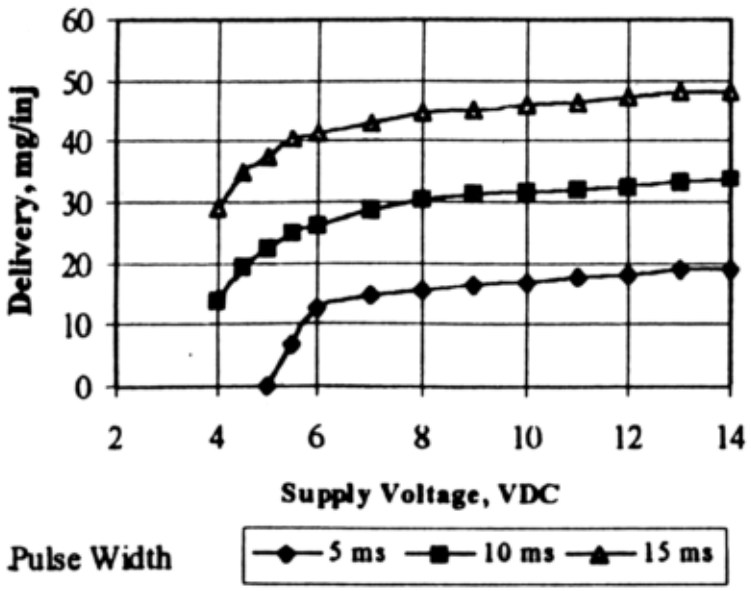

4.4 Engine Control Module (ECM)

4.4.1 Motec ECM Description

The Motec is a programmable ECM which allows for immediate tuning adjustments on the fly while the engine operating. This unit will be used to develop timing and injection maps during engine dynamometer testing. Because of its “on-the-fly” tuning capability, parameters can be adjusted while the engine is running to optimize emissions, fuel economy, and/or power. Once the optimal operating strategy is developed, electronics will be fabricated to operate the engine without the need for the Motec.

4.4.2 Ignition Timing

Experiments have shown that at a constant A/F ratio, timing advance is not as sensitive for engines operating on hydrogen as it is for engines operating on gasoline. However, as the A/F ratio varies, timing advance becomes very important for hydrogen engines. The primary reason is that the deflagration rate for hydrogen increases very quickly relative to gasoline as the A/F goes

from a lean mixture to a rich mixture. For instance, at a very lean A/F ratio, the burning velocity of hydrogen is similar to that of gasoline. However, at a stoichiometric mixture of hydrogen and air, the burning velocity of hydrogen is almost 10 times that of gasoline. To compensate for this, the Motec will be programmed not only to adjust timing based on engine speed, temperature, and power, but also A/F ratio. These timing maps will be developed in Phase III during engine dynamometer testing.

4.4.3 Injection Timing and Duration

Injection timing and duration will be based primarily on inputs from the Mass Air Flow (MAF) and tachometer sensor. The Motec will take these inputs and determine the appropriate injection time and PW to yield the desired A/F ratio. Feedback from the Exhaust Gas Oxygen (EGO) sensor will provide fine tuning the PW. Injector time delays (the time it takes for the injector to fully open after it has been energized) at various pressure will be programmed into the Motec. This will ensure that the fuel is entering the manifold at the proper time. Injector time delay as a function of rail pressure was also developed during this phase of the project.

4.4.4 Safety Considerations

Safety considerations will also be programmed into the ECM to minimize potential safety hazards. For instance, on engine start-up, there will be a slight delay in ignition spark during engine cranking to exhaust any hydrogen that may have accumulated in the combustion chamber. On engine shutdown, the injectors will be shutdown prior to terminating the ignition spark. This will allow the combustion chamber to be fully exhausted of hydrogen before the engine is completely stopped. Another feature that will be incorporated into the ECM is a program that will shut down an injector if its corresponding cylinder loses its spark. This will prevent unburned hydrogen from entering the exhaust system.

4.5 Battery Balance

Battery performance is a major roadblock to successful electric vehicle commercialization. Balancing of battery SOC's increases battery life. Automated balancing circuitry will decrease overcharging (and gassing) and decrease manual maintenance.

Under Task 6 of this project, CE-CERT is investigating electronic means of controlling the charging process to automatically improve battery balance. The Task has been subdivided into four subtasks:

> ***Task 6.1 Literature Survey—***A review of the literature was performed to identify existing automated battery balance techniques and their strengths and weaknesses.
>
> ***Task 6.2 Design Prototype Battery Bypass Circuit—***A prototype circuit was designed for use with the 18 six-volt batteries on an electric Ford Escort currently in use at CE-CERT.
>
> ***Task 6.3 Implement and Test Prototype Battery Bypass Circuit—***The prototype circuit was implemented and tested in the laboratory to verify its operation and power dissipation specifications, prior to on-vehicle use.

Task 6.4 Implement and Test Battery Bypass Circuit on an EV—The prototype circuit was implemented and tested on eight batteries of the series string. Voltages on all eighteen batteries were recorded for analysis and comparison.

4.6 Energy Management

Since an HEV has multiple power sources (e.g., batteries, APU), strategies are necessary to specify how to best satisfy the instantaneous power demand from the various sources. Under this task, CE-CERT designed, developed, and evaluated different energy management strategies for use in the HEV testbed (HEVT).

Task 7.1 Literature Survey—The objective of the energy management system is to meet the drivetrain power requirements while minimizing fuel usage and emissions. A detailed review of existing energy management techniques for series HEVs has been completed and is reviewed in the next section.

Task 7.2 Modeling and Simulation—An HEV model and dynamic simulation was developed to allow analysis of alternative energy management strategies.

Task 7.3 HEV Energy Management Design—An energy management system was designed for the simulated vehicle.

Task 7.4 Energy Management Implementation and Testing—The energy management system designed in Task 7.4 was implemented and tested in the simulation developed in Task 7.2.

5.0 Results

5.1 Injector Dynamic Flow Characteristics

Due to the high speed at which the injectors open and close and the low flow rate for each opening, it is impossible to measure the flow rate per injection directly. To determine the mass of hydrogen per injection the following logic was used:

Each injector flow test was repeated 4 times at PW's of 4, 6, 8, 10, 12, 14, and 16 ms. A 50% duty was chosen so that the hydrogen flow rate for each test would remain fairly constant for each PW (even though the injector is open 4 times longer for a PW of 16 ms compared to a PW of 4 ms, for a duty cycle of 50%, it is also closed 4 times longer). In this way if the operator noticed a large variance in flow he could verify everything is operating correctly before continuing with the next test.

The following test data was measured and recorded at a rate of approximately 10 samples per second:

Exact time (sec)
Hydrogen flow rate (lb./min)
Manifold rail pressure (psia)
Hydrogen temperature (°C)

A typical test consisted of adjusting the PW modulator to the proper PW (as displayed on the Tektronix 5112 Dual Beam Oscilloscope), starting the data acquisition system, initiating injection firing, terminating injection firing after 25 seconds, and stopping data acquisition at 30 seconds. This was repeated four times for each PW. Each test yielded approximately 300 data points. A typical plot of this data is shown in **Figure 5-1.** Data from each test was then analyzed.

To eliminate the perturbations in the flow rate due to the initiation and termination of flow at the beginning and the end of each test, only 10 to 20 seconds (test duration) of the steady-state flow during the middle of the test was used. The average flow rate during this period was multiplied by the test duration to yield the total mass of hydrogen that pass through the injector. Knowing the test duration and the frequency at which the injectors are being operated, the number of injections can be calculated. This value is then divided into the total mass to yield the flow rate (mg/inj). This protocol was repeated for pressures of 25, 50, 75, 100, 125, 150, 175, and 200 psig for injectors SP-014 and SP-021. For injector SP-051, pressures of 50, 100, 150, and 200 psig were used. It was found that the SP-010 injector would not open at 200 psig and performed poorly at 150 psig. The SP-010 was therefore only tested at 50 and 100 psig. The data analysis sheets for these tests can be found in **Appendix A, B, C, and D**. A summary of the flow rate, standard deviation in flow rate and inlet pressure relative to PW is listed in **Tables 5-1, 5-2, 5-3, and 5-4** for the SP-014, SP-021, SP-051, and SP-010 injectors, respectively.

Figure 5-1. A typical plot of flow rate and pressure vs. time.

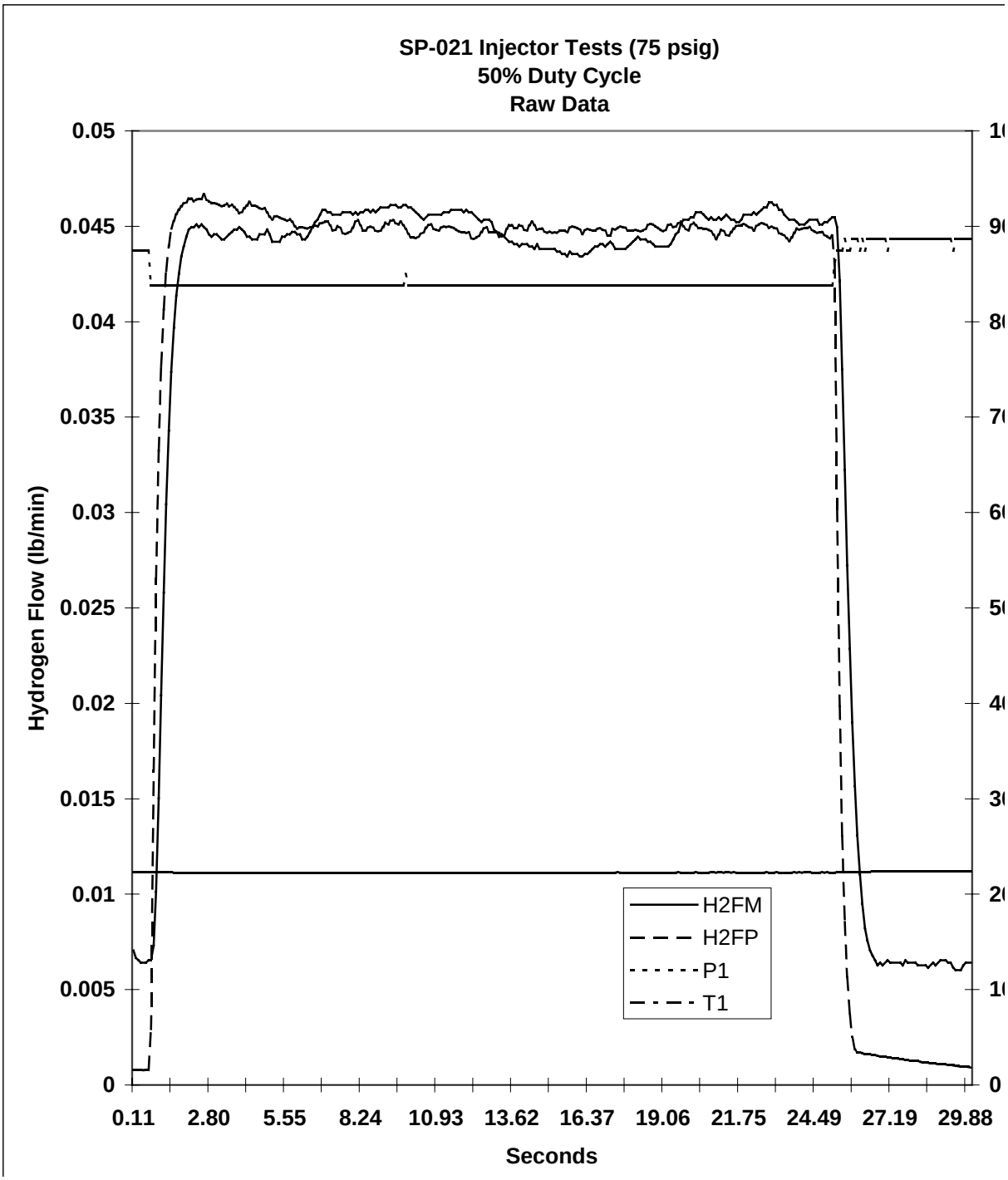

The average flow rates calculated from the data summary in **Appendices A, B, C, and D** are plotted versus PW at each pressure and are shown in **Appendices E, F, G, and H**, for SP-014, SP-021, SP-051, and SP-010, respectively. The flow rate curves at various pressures in **Appendix E, F, G, and H** are incorporated into the graphs in **Figures 5-2, 5-3, 5-4, and 5-5.**

From Tables 5-1 to 5-4 and Figures 5-2 to 5-5, it can be seen that a wide range of flows are possible by changing PW and rail pressures. It is also evident that the injectors provide precise, stable, and reliable metering of the hydrogen gas.

5.2 Injector Dynamic Response Characteristics

Response time of a solenoid depends upon the physical size of the solenoid, power input, drive circuit, mass and travel of armature, and load. The opening time of the injector, which is the time required for the armature to reach its fully opened position after initiation of the drive circuit pulse input, depends upon the gas supply pressure. The closing time, also depends on supply pressure. Since it is more important to know when flow actually starts than when the injector in physically open, it was decided to measure the pressure at the outlet of the injector instead of trying to measure position of the injector ball poppet. To accomplish this measurement, a piezoelectric pressure transducer was installed at the outlet of injector.

During data collection, the rail pressure and the PW remained constant for each test. The rail pressure was controlled using a pressure regulator (PR1 shown in **Figure 4-1**) on the supply tanks. Data was recorded by feeding both signals from the oscilloscope into a Keithly Metrabyte Model DAS16 100,000 samples per second analog and digital I/O board interfaced with a 100 MHz Pentium computer. A program called Streamer was used to record the amplitude of each wave form at 30 KHz relative to the amplitude of the previous sample.

A typical plot of pressure rise and PW voltage versus time in shown in **Figure 5-6.** The time delay (the time it takes for the pressure to reach 50% of its final pressure after the PW signal is sent) is the start of the square wave to the midpoint of the first large peak of the pressure signal. For each pressure and PW, three to five cycles (injection firings) were measured and recorded. Plot of the pressure and PW profiles for each of these runs were made by overlaying each of these runs relative to injection firing (initial rise in the PW profile). Because the amplitude for the PW and pressure profiles are not required for the calculations to determine the time delays, the computer units were not converted to engineering units. **Table 5-5** and **5-6** lists the results of these tests for the SP-014 and SP-021 injectors, respectively. It can be seen from these tables that the SP-021 injector opens about 1 ms faster than the SP-014 injector. This is mainly due to the larger poppet ball (more mass) and the larger orifice (more surface area for the pressurize gas to force the valve closed) of the SP-014 injector. In addition, it can be seen from these tables that the time the injector is open is less than the PW signal. The injector is considered open from the time when 50% of flow is reached to the time the flow drops to 50%. It is also assumed that flow is directly related to pressure. For the SP-014 injector, it is about 2 ms less and for the SP-021 it is about 1 ms less. This is important information for programming the ECM. For example, at an engine speed of 5,000 rpm , the injector only has 4.8 ms to inject the hydrogen (see Section 4.2). For the SP-014 injector, the ECM therefore would send a 6.8 ms PW so that the injector would be open for 4.8 ms (6.8 ms - 2 ms). Likewise, if it was the SP-021 injector, the ECM would send a 5.8 ms PW signal (5.8 ms -1 ms). The SP-051 and SP-010 injectors were not evaluated for response time due to time constraints.

Table 5-1. SP-014 injector summary.

	Flow rate (mg/injection)						517_14A	
Pulse Width (ms)	Run 1	Run 2	Run 3	Run 4	AVG Q	ST DEV	% DEV	AVG PSIA
4	1.22	1.22	1.22	1.22	1.22	0.0021	0.17%	35
6	1.54	1.54	1.55	1.55	1.54	0.0061	0.39%	36
8	2.11	2.10	2.11	2.10	2.11	0.0020	0.10%	36
10	2.55	2.55	2.56	2.55	2.55	0.0041	0.16%	36
12	2.90	2.89	2.89	2.86	2.88	0.0162	0.56%	36
14	3.32	3.32	3.31	3.31	3.32	0.0067	0.20%	35
16	3.71	3.72	3.72	3.73	3.72	0.0088	0.24%	35
	Flow rate (mg/injection)						511_14B	
Pulse Width (ms)	Run 1	Run 2	Run 3	Run 4	AVG Q	ST DEV	% DEV	AVG PSIA
4	2.73	2.75	2.76	2.77	2.75	0.0169	0.61%	58
6	3.37	3.23	3.45	3.46	3.38	0.1082	3.20%	58
8	4.41	4.50	4.65	4.61	4.54	0.1066	2.35%	59
10	5.61	5.69	5.78	5.74	5.71	0.0716	1.25%	59
12	6.49	6.49	6.53	6.51	6.51	0.0156	0.24%	60
14	7.38	7.32	7.32	7.43	7.36	0.0555	0.75%	60
16	8.11	8.29	8.17	8.34	8.23	0.1043	1.27%	61
	Flow rate (mg/injection)						510_14C	
Pulse Width (ms)	Run 1	Run 2	Run 3	Run 4	AVG Q	ST DEV	% DEV	AVG PSIA
4	3.86	3.88	3.85	3.87	3.86	0.0114	0.29%	83
6	5.10	5.07	5.10	5.11	5.09	0.0163	0.32%	84
8	6.14	6.10	6.22	6.22	6.17	0.0603	0.98%	83
10	7.64	7.71	7.71	7.74	7.70	0.0428	0.56%	83
12	8.56	8.69	8.66	8.67	8.64	0.0584	0.68%	84
14	9.96	10.02	9.99	10.01	9.99	0.0296	0.30%	84
16	11.27	11.37	11.31	11.37	11.33	0.0512	0.45%	84
	Flow rate (mg/injection)						604_14D	
Pulse Width (ms)	Run 1	Run 2	Run 3	Run 4	AVG Q	ST DEV	% DEV	AVG PSIA
4	4.61	4.56	4.55	4.47	4.55	0.0594	1.31%	108
6	5.42	5.41	5.40	5.41	5.41	0.0066	0.12%	109
8	7.46	7.52	7.55	7.57	7.52	0.0489	0.65%	110
10	9.12	9.06	9.05	9.05	9.07	0.0334	0.37%	110
12	10.53	10.56	10.50	10.51	10.53	0.0234	0.22%	111
14	12.09	12.05	12.05	12.04	12.06	0.0235	0.20%	110
16	13.61	13.57	13.68	13.71	13.64	0.0675	0.49%	110
	Flow rate (mg/injection)						521_14E	
Pulse Width (ms)	Run 1	Run 2	Run 3	Run 4	AVG Q	ST DEV	% DEV	AVG PSIA
4	4.40	4.37	4.33	4.32	4.35	0.0351	0.81%	134
6	6.40	6.41	6.41	6.41	6.41	0.0038	0.06%	133
8	8.08	8.08	8.06	8.05	8.07	0.0133	0.17%	134
10	9.91	9.96	9.97	10.06	9.97	0.0600	0.60%	134
12	12.02	12.02	12.03	12.02	12.02	0.0041	0.03%	133
14	13.90	13.94	13.96	13.97	13.94	0.0317	0.23%	133
16	15.96	15.98	15.94	15.94	15.96	0.0191	0.12%	134
	Flow rate (mg/injection)						521_14F	
Pulse Width (ms)	Run 1	Run 2	Run 3	Run 4	AVG Q	ST DEV	% DEV	AVG PSIA
4	5.05	5.05	5.03	5.03	5.04	0.0117	0.23%	157
6	6.63	6.63	6.62	#REF!	6.63	0.0043	0.07%	158
8	9.02	9.03	9.01	8.82	8.97	0.0994	1.11%	158
10	11.37	11.43	11.32	11.36	11.37	0.0480	0.42%	158
12	13.56	13.55	13.53	13.54	13.54	0.0120	0.09%	158
14	16.16	16.12	16.06	16.16	16.12	0.0445	0.28%	158
16	19.13	19.12	19.11	19.07	19.11	0.0281	0.15%	159
	Flow rate (mg/injection)						531_14G	
Pulse Width (ms)	Run 1	Run 2	Run 3	Run 4	AVG Q	ST DEV	% DEV	AVG PSIA
4	5.94	5.92	5.93	5.96	5.94	0.0178	0.30%	184
6	7.56	7.56	7.56	7.53	7.55	0.0122	0.16%	184
8	10.09	10.11	10.12	10.09	10.10	0.0112	0.11%	184
10	12.56	12.64	12.56	12.58	12.58	0.0378	0.30%	185
12	15.52	15.50	15.36	15.30	15.42	0.1065	0.69%	185
14	18.20	18.17	18.12	18.10	18.15	0.0473	0.26%	184
16	20.76	20.70	20.68	20.48	20.66	0.1190	0.58%	183
	Flow rate (mg/injection)						531_14H	
Pulse Width (ms)	Run 1	Run 2	Run 3	Run 4	AVG Q	ST DEV	% DEV	AVG PSIA
4	6.04	5.99	6.00	5.96	6.00	0.0334	0.56%	208
6	7.67	7.69	7.68	7.69	7.68	0.0053	0.07%	209
8	10.61	10.62	10.64	10.63	10.63	0.0138	0.13%	210
10	13.54	13.51	13.53	13.55	13.53	0.0157	0.12%	210
12	16.66	16.65	16.64	16.64	16.65	0.0094	0.06%	210
14	19.74	19.72	19.72	19.74	19.73	0.0105	0.05%	209
16	22.40	22.42	22.39	22.40	22.40	0.0130	0.06%	209

Table 5-2. SP-021 injector summary.

	Flow rate (mg/injection)						517_21A	
Pulse Width (ms)	Run 1	Run 2	Run 3	Run 4	AVG Q	ST DEV	% DEV	AVG PSIA
4	1.23	1.23	1.23	1.23	1.23	0.0023	0.19%	36
6	1.54	1.55	1.55	1.55	1.54	0.0049	0.32%	36
8	2.11	2.11	2.10	2.11	2.11	0.0049	0.23%	36
10	2.54	2.55	2.56	2.56	2.55	0.0095	0.37%	36
12	2.87	2.90	2.90	2.90	2.89	0.0145	0.50%	36
14	3.32	3.34	3.34	3.32	3.33	0.0105	0.31%	36
16	3.70	3.72	3.72	3.72	3.71	0.0093	0.25%	35
	Flow rate (mg/injection)						511_21B	
Pulse Width (ms)	Run 1	Run 2	Run 3	Run 4	AVG Q	ST DEV	% DEV	AVG PSIA
4	2.02	2.01	2.03	2.03	2.02	0.0080	0.40%	59
6	2.62	2.64	2.64	2.63	2.63	0.0077	0.29%	60
8	3.28	3.30	3.30	3.31	3.30	0.0106	0.32%	60
10	3.99	4.00	4.00	4.02	4.01	0.0132	0.33%	60
12	4.73	4.78	4.73	4.73	4.74	0.0251	0.53%	61
14	5.42	5.47	5.48	5.47	5.46	0.0277	0.51%	61
16	6.18	6.23	6.24	6.18	6.21	0.0327	0.53%	61
	Flow rate (mg/injection)						510_21C	
Pulse Width (ms)	Run 1	Run 2	Run 3	Run 4	AVG Q	ST DEV	% DEV	AVG PSIA
4	2.72	2.68	2.67	2.67	2.69	0.0206	0.77%	84
6	3.19	3.20	3.19	3.19	3.19	0.0038	0.12%	85
8	4.20	4.21	4.22	4.20	4.21	0.0065	0.15%	85
10	5.28	5.30	5.30	5.27	5.29	0.0135	0.26%	84
12	6.35	6.35	6.36	6.38	6.36	0.0159	0.25%	85
14	7.45	7.47	7.48	7.51	7.48	0.0231	0.31%	85
16	8.36	8.46	8.48	8.47	8.44	0.0547	0.65%	85
	Flow rate (mg/injection)						524_21D	
Pulse Width (ms)	Run 1	Run 2	Run 3	Run 4	AVG Q	ST DEV	% DEV	AVG PSIA
4	2.88	2.88	2.88	2.86	2.87	0.0065	0.23%	111
6	4.26	4.27	4.27	4.28	4.24	0.0145	0.34%	112
8	5.44	5.46	5.45	5.45	5.45	0.0034	0.06%	112
10	6.81	6.83	6.83	6.83	6.67	0.1291	1.94%	111
12	7.79	7.77	7.79	7.77	7.79	0.0138	0.18%	111
14	9.19	9.14	9.17	9.13	9.20	0.0162	0.18%	111
16	10.30	10.28	10.28	10.28	10.26	0.0107	0.10%	111
	Flow rate (mg/injection)						521_21E	
Pulse Width (ms)	Run 1	Run 2	Run 3	Run 4	AVG Q	ST DEV	% DEV	AVG PSIA
4	3.49	3.47	3.45	3.45	3.46	0.0196	0.57%	135
6	4.43	4.44	4.42	4.43	4.43	0.0093	0.21%	134
8	5.96	6.02	6.01	5.97	5.99	0.0274	0.46%	134
10	7.56	7.46	7.44	7.45	7.48	0.0553	0.74%	135
12	9.01	9.02	9.03	8.99	9.01	0.0185	0.21%	134
14	10.40	10.43	10.42	10.42	10.41	0.0136	0.13%	134
16	11.95	11.97	11.99	11.98	11.97	0.0138	0.12%	134
	Flow rate (mg/injection)						521_21F	
Pulse Width (ms)	Run 1	Run 2	Run 3	Run 4	AVG Q	ST DEV	% DEV	AVG PSIA
4	3.99	3.97	3.97	3.94	3.97	0.0233	0.59%	158
6	5.07	5.03	5.03	5.03	5.04	0.0189	0.38%	159
8	6.81	6.80	6.80	6.79	6.80	0.0098	0.14%	159
10	8.44	8.44	8.44	8.42	8.43	0.0066	0.08%	158
12	10.20	10.21	10.21	10.19	10.20	0.0089	0.09%	159
14	12.15	12.20	12.19	12.22	12.19	0.0288	0.24%	159
16	13.82	13.90	13.93	13.96	13.90	0.0606	0.44%	159
	Flow rate (mg/injection)						531_21G	
Pulse Width (ms)	Run 1	Run 2	Run 3	Run 4	AVG Q	ST DEV	% DEV	AVG PSIA
4	4.10	4.04	3.99	3.98	4.02	0.0549	1.36%	187
6	5.75	5.78	5.77	5.77	5.77	0.0138	0.24%	185
8	7.50	7.44	7.42	7.42	7.45	0.0366	0.49%	185
10	9.41	9.41	9.40	9.38	9.40	0.0129	0.14%	186
12	11.72	11.72	11.71	11.71	11.71	0.0054	0.05%	185
14	13.80	13.79	13.76	13.77	13.78	0.0197	0.14%	185
16	15.77	15.68	15.55	15.96	15.74	0.1748	1.11%	183
	Flow rate (mg/injection)						611_21H	
Pulse Width (ms)	Run 1	Run 2	Run 3	Run 4	AVG Q	ST DEV	% DEV	AVG PSIA
4	4.28	4.31	4.32	4.34	4.31	0.0219	0.51%	208
6	5.90	5.91	5.89	5.88	5.89	0.0092	0.16%	209
8	8.26	8.28	8.28	8.22	8.26	0.0270	0.33%	209
10	10.35	10.34	10.39	10.35	10.36	0.0202	0.19%	209
12	12.99	12.97	12.96	12.93	12.96	0.0224	0.17%	208
14	15.31	15.28	15.23	15.23	15.27	0.0396	0.26%	208
16	17.60	17.62	17.61	17.61	17.61	0.0104	0.06%	208

Table 5-3. SP-051 injector summary

	Flow rate (mg/injection)						807_51B	
Pulse Width (ms)	Run 1	Run 2	Run 3	Run 4	AVG Q	ST DEV	% DEV	AVG PSIA
4	1.56	1.55	1.54	1.54	1.55	0.0094	0.0061	62
6	2.21	2.21	2.20	2.20	2.21	0.0031	0.0014	62
8	2.79	2.79	2.78	2.79	2.79	0.0058	0.0021	61
10	3.36	3.37	3.36	3.37	3.37	0.0084	0.0025	61
12	4.01	4.01	4.02	4.02	4.01	0.0083	0.0021	61
14	4.62	4.63	4.63	4.63	4.62	0.0061	0.0013	61
16	5.24	5.25	5.26	5.26	5.25	0.0080	0.0015	61
	Flow rate (mg/injection)						807_51D	
Pulse Width (ms)	Run 1	Run 2	Run 3	Run 4	AVG Q	ST DEV	% DEV	AVG PSIA
4	2.91	2.91	2.89	2.88	2.90	0.0152	0.0053	110
6	3.50	3.52	3.53	3.51	3.52	0.0100	0.0028	110
8	4.68	4.66	4.68	4.68	4.67	0.0076	0.0016	110
10	5.77	5.78	5.78	5.78	5.78	0.0041	0.0007	110
12	6.85	6.86	6.86	6.84	6.86	0.0094	0.0014	110
14	7.95	7.99	7.99		7.98	0.0227	0.0028	110
16		9.12	9.14	9.14	9.13	0.0127	0.0014	111
	Flow rate (mg/injection)						807_51F	
Pulse Width (ms)	Run 1	Run 2	Run 3	Run 4	AVG Q	ST DEV	% DEV	AVG PSIA
4	3.46	3.45	3.46	3.48	3.46	0.0137	0.0039	159
6	4.69	4.70	4.76	4.70	4.71	0.0314	0.0067	159
8	6.20	6.23	6.26	6.26	6.24	0.0248	0.0040	159
10	7.81	7.83	7.84	7.84	7.83	0.0157	0.0020	159
12	9.47	9.54	9.53		9.51	0.0396	0.0042	159
14	11.02	11.06	11.09	11.07	11.06	0.0296	0.0027	159
16	12.78	12.79	12.81	12.83	12.80	0.0216	0.0017	159
	Flow rate (mg/injection)						807_51H	
Pulse Width (ms)	Run 1	Run 2	Run 3	Run 4	AVG Q	ST DEV	% DEV	AVG PSIA
4	4.49	4.45	4.44	4.48	4.46	0.0247	0.0055	210
6	5.88	5.83	5.79	5.83	5.83	0.0383	0.0066	211
8	7.74	7.76	7.76	7.75	7.75	0.0094	0.0012	211
10	9.88	9.87	9.89	9.87	9.88	0.0120	0.0012	210
12	12.14	12.13	12.16	12.13	12.14	0.0145	0.0012	210
14	14.33	14.34	14.36	14.34	14.34	0.0127	0.0009	210
16	16.46	16.47	16.44	16.46	16.46	0.0108	0.0007	210

Table 5-4. SP-010 injector summary.

	Flow rate (mg/injection)						918_10B	
Pulse Width (ms)	Run 1	Run 2	Run 3	Run 4	AVG Q	ST DEV	% DEV	AVG PSIA
4	6.69	6.21	6.06	6.04	6.25	0.3017	0.0298	59
6	8.82	8.79	8.78	8.79	8.80	0.0175	0.0119	59
8	11.93	11.95	11.94	11.95	11.94	0.0094	0.0125	59
10	14.68	14.73	14.64	14.64	14.67	0.0418	0.0125	60
12	17.21	17.20	17.13	17.12	17.17	0.0460	0.0131	59
14	19.63	19.63	19.64	19.68	19.65	0.0205	0.0126	59
16	22.08	22.14	22.09	22.10	22.10	0.0231	0.0120	60
	Flow rate (mg/injection)						918_10D	
Pulse Width (ms)	Run 1	Run 2	Run 3	Run 4	AVG Q	ST DEV	% DEV	AVG PSIA
4	7.70	7.59	7.41	7.44	7.53	0.1363	0.0462	110
6	12.22	12.27	12.14	12.17	12.20	0.0557	0.0295	110
8	18.33	18.43	18.40	18.33	18.37	0.0492	0.0196	109
10	23.53	23.43	23.38	23.36	23.42	0.0746	0.0199	109
12	28.16	28.12	28.04	28.04	28.09	0.0624	0.0186	109
14	32.65	32.61	32.50	32.50	32.56	0.0756	0.0197	108
16	37.18	37.20	37.24	37.22	37.21	0.0259	0.0183	108

Figure 5-2. Flow rate at various pressures vs. PW (ms) for the SP-014 injector.

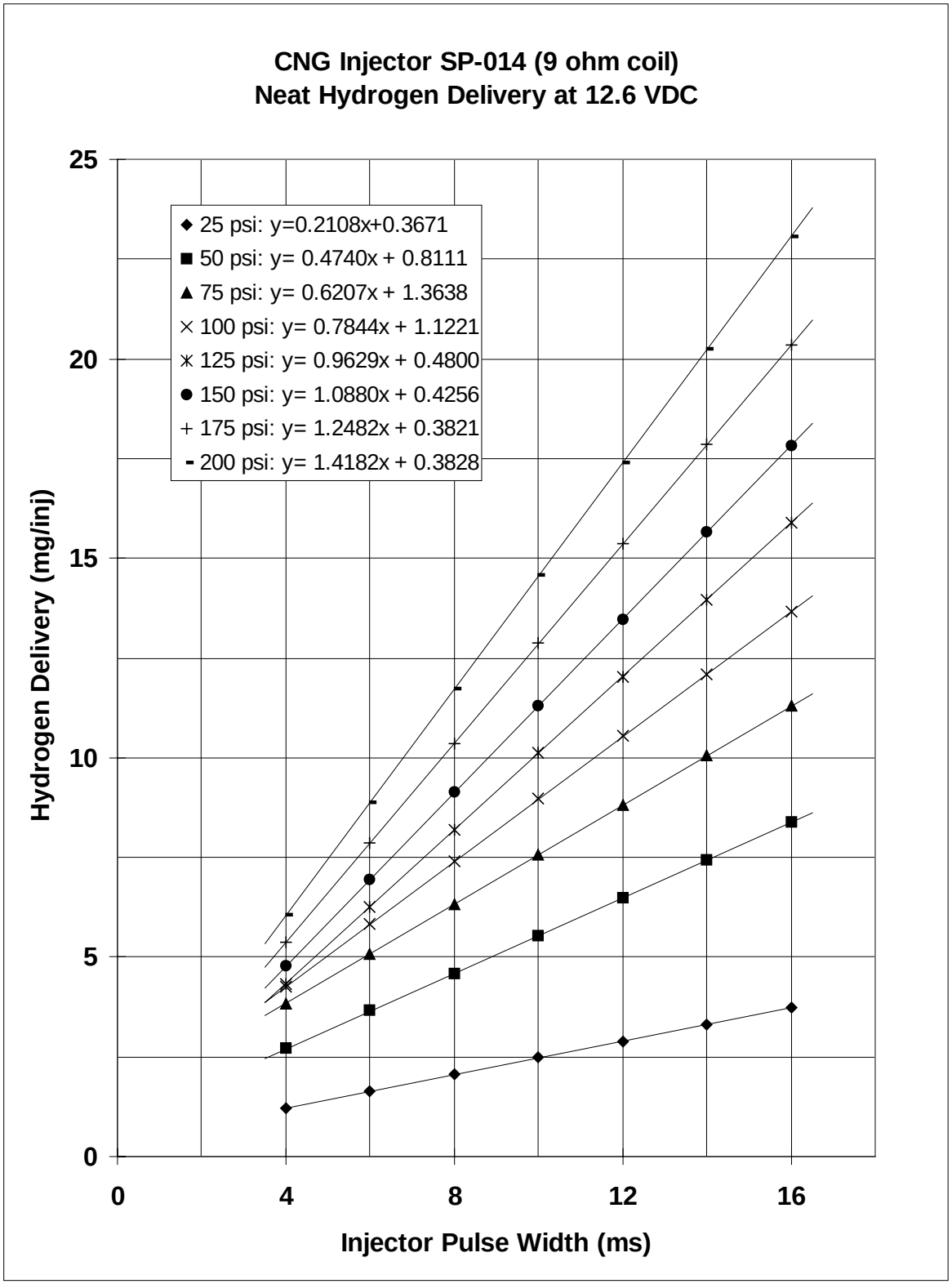

Figure 5-3. Flow rate at various pressures vs. PW (ms) for the SP-021 injector.

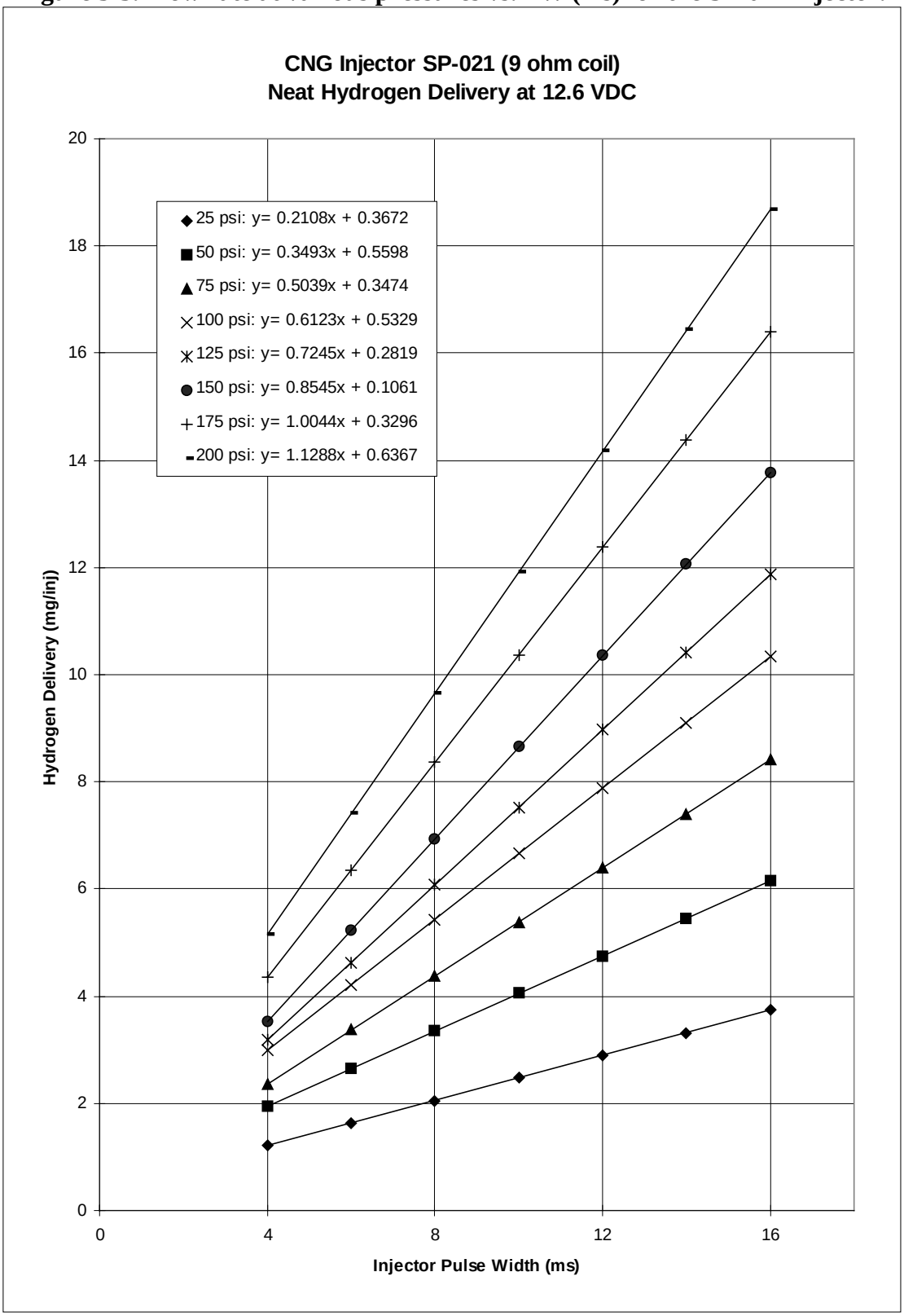

Figure 5-4. Flow rate at various pressures vs. PW (ms) for the SP-051 injector.

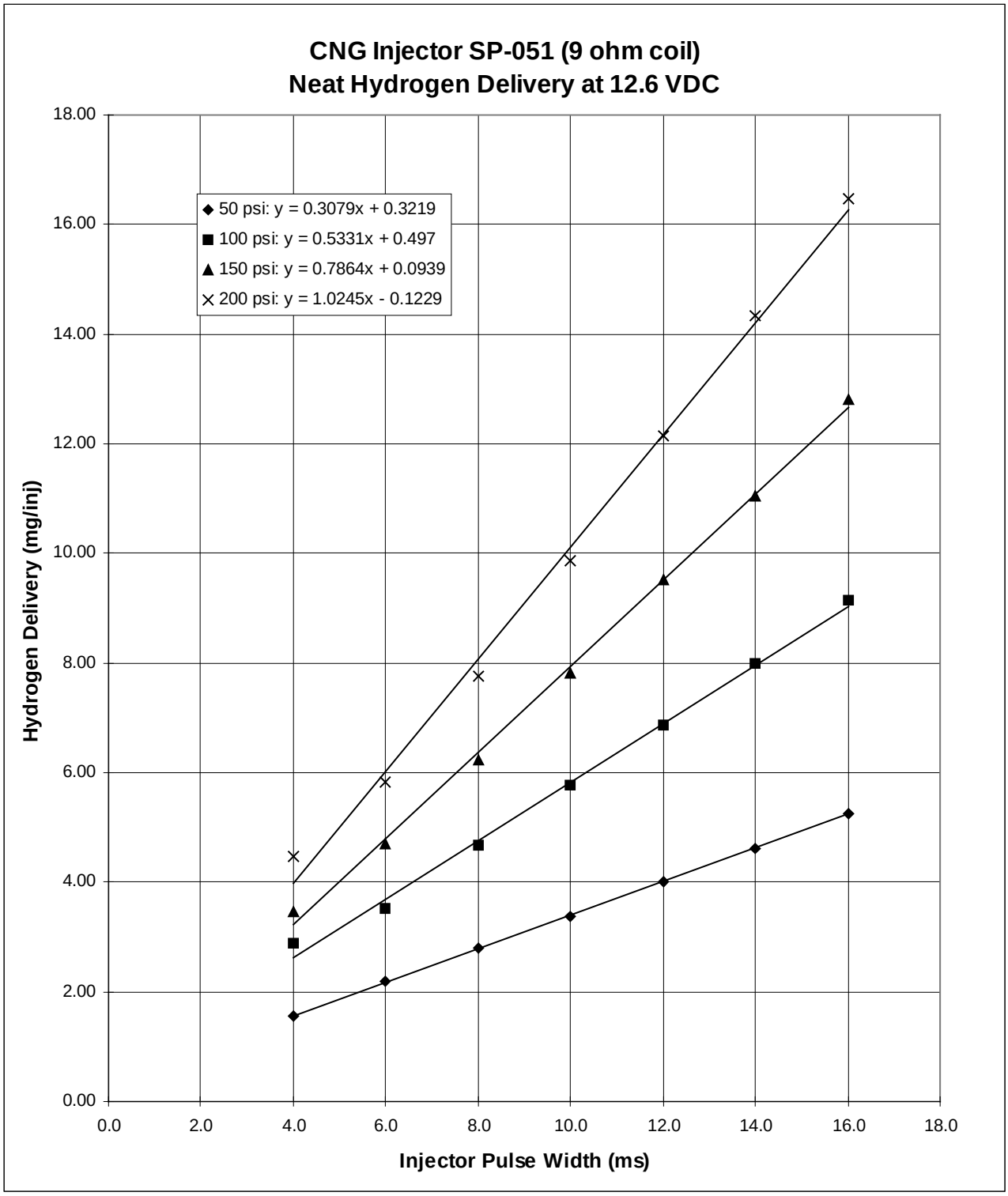

Figure 5-5. Flow rate at various pressures vs. PW (ms) for the SP-010 injector.

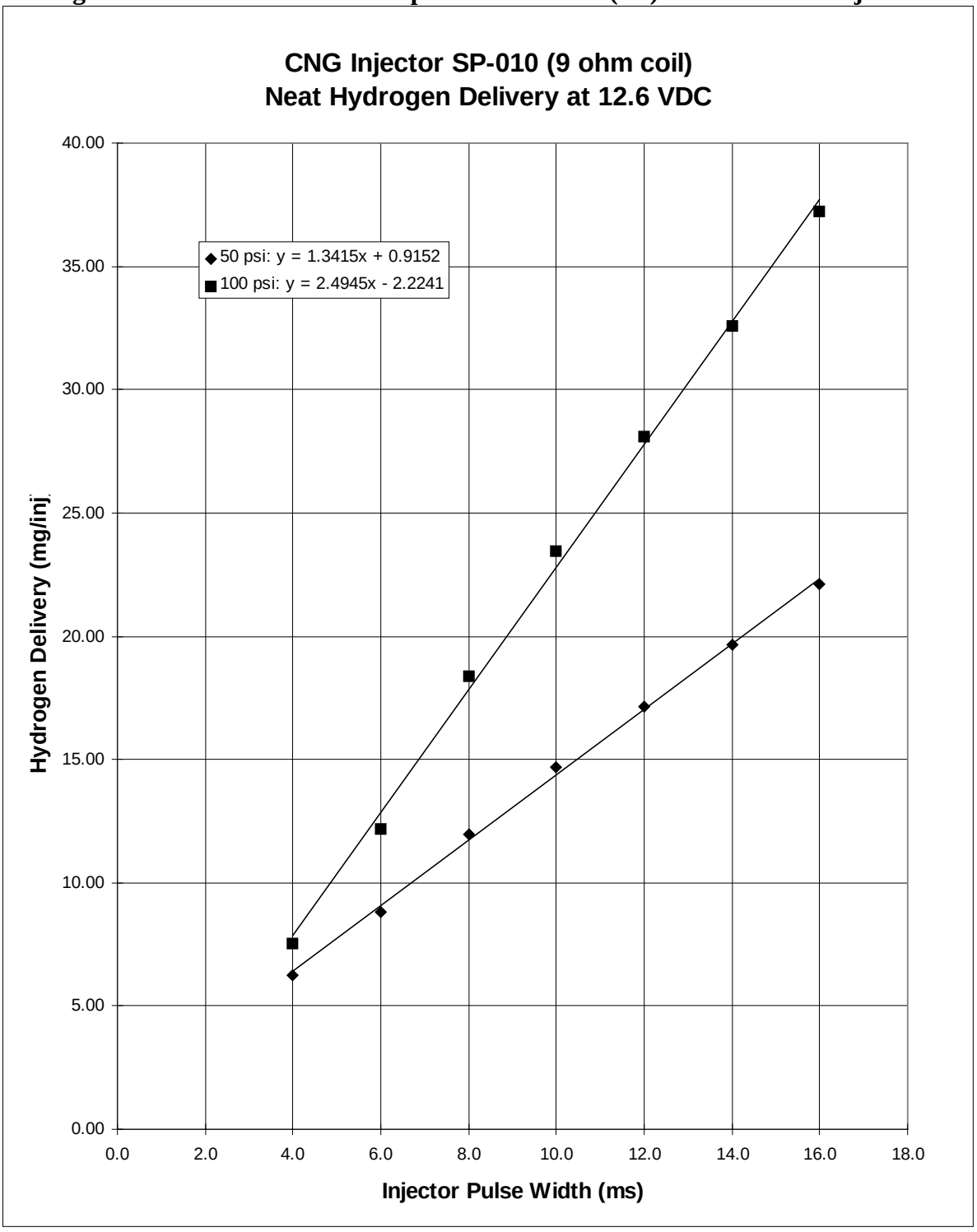

Injector time delay was measured by finding the time difference between the start of the square wave signal until the first time the pressure signal crosses the average "open pressure" of the injector. This point was chosen because from that point on the average flow can be assumed to be the "open pressure" value of the injector. A complete set of time delay plots for SP-014 and SP-

021 can be found in **Appendix I** and **J,** respectively. The time delays found in **Appendix I** and **J** are plotted relative to pressures to give a characteristic curve of the time delay as a function of rail pressure. These curves for SP-014 and SP-021 are shown in **Figure 5-7**. From **Figure 5-7** it can be seen that the delay time can vary from 2.6 ms at 25 psig to 4.0 ms at 200 psig for the SP-014 injector and 2.3 ms at 25 psig to 3.0 ms at 200 psig for the SP-021 injector. These delay times will be useful in programming the injector trigger time in the ECM. For example, if the rail pressure is at 200 psia, and it is desired to have hydrogen injection started at 1 ms ATDC, the ECM will send a signal to trigger the SP-014 injector 4.0 ms before the injector actually needs to be fully opened. For this example, the ECM will trigger the injector at 3.0 ms BTDC (4.0 - 1 ms).

5.3 Injector Leakage Characteristics

The leakage flow rates for the four BKM injector models were quite low. The flow rates were so slow it was determined that the escaped hydrogen gas was insignificant and will most likely not cause any problems. Of all the injectors, the SP-051 injector displayed the highest leakage rate at 200 psig (approximately 250 cc/min). It was also observed that each time an injector was run for a brief period of time, the leakage rates decreased. This is most likely due to the poppet ball inside the injector becoming better seated after each run. A plot displaying the leakage rates for all four injectors can be found in **Figure 5-8**.

Figure 5-6. Pressure rise and PW signal vs. time.

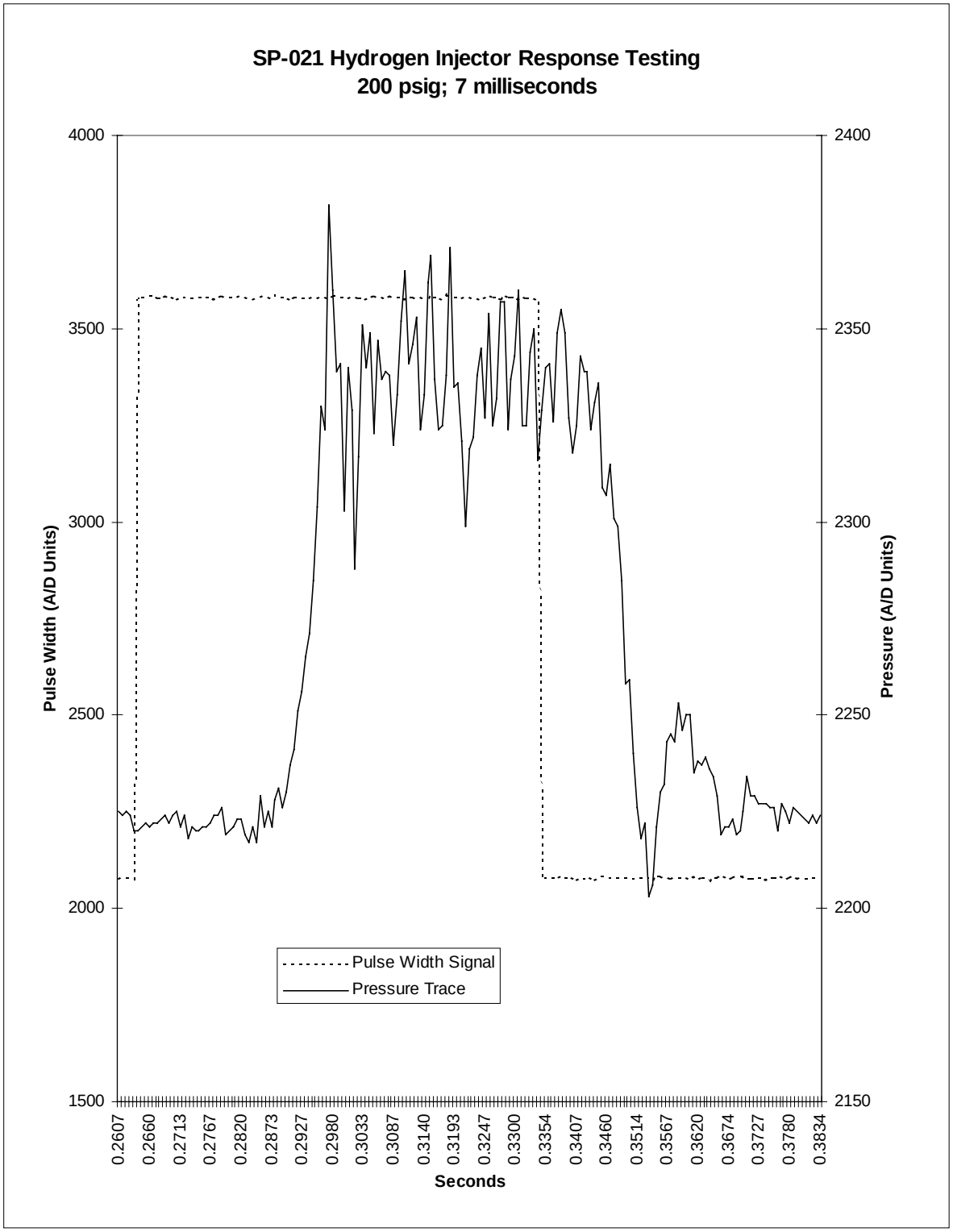

Table 5-5. SP-014 injector dynamic characteristics.

SP-014 @ 200 psig				
PW Setting (ms)	Actual PW (ms)	Time Delay (ms)	Valve Open (ms)	Delta (ms)
4	4.07	4.1	1.9	2.1
5	5.07	3.9	3.5	1.6
6	6.07	3.9	3.9	2.1
7	7	4	5	2
8	8.06	4	6	2.1
12	12.06	4	10.1	1.9
16	16.13	3.9	13.7	2.5
Average =		4.0		2.0

Table 5-6. SP-021 injector dynamic characteristics.

SP-014 @ 200 psig				
PW Setting (ms)	Actual PW (ms)	Time Delay (ms)	Valve Open (ms)	Delta (ms)
4	3.9	3	2.8	1.1
5	5	3	3.5	1.5
6	6.06	3	4.2	1.9
7	6.96	3	5.6	1.4
8	7.72	3	6.3	1.4
12	11.61	3	10.4	1.3
16	15.51	3	14.3	1.3
Average =		3.0		1.4

Figure 5-7. Injector opening time delay vs. inlet pressure.

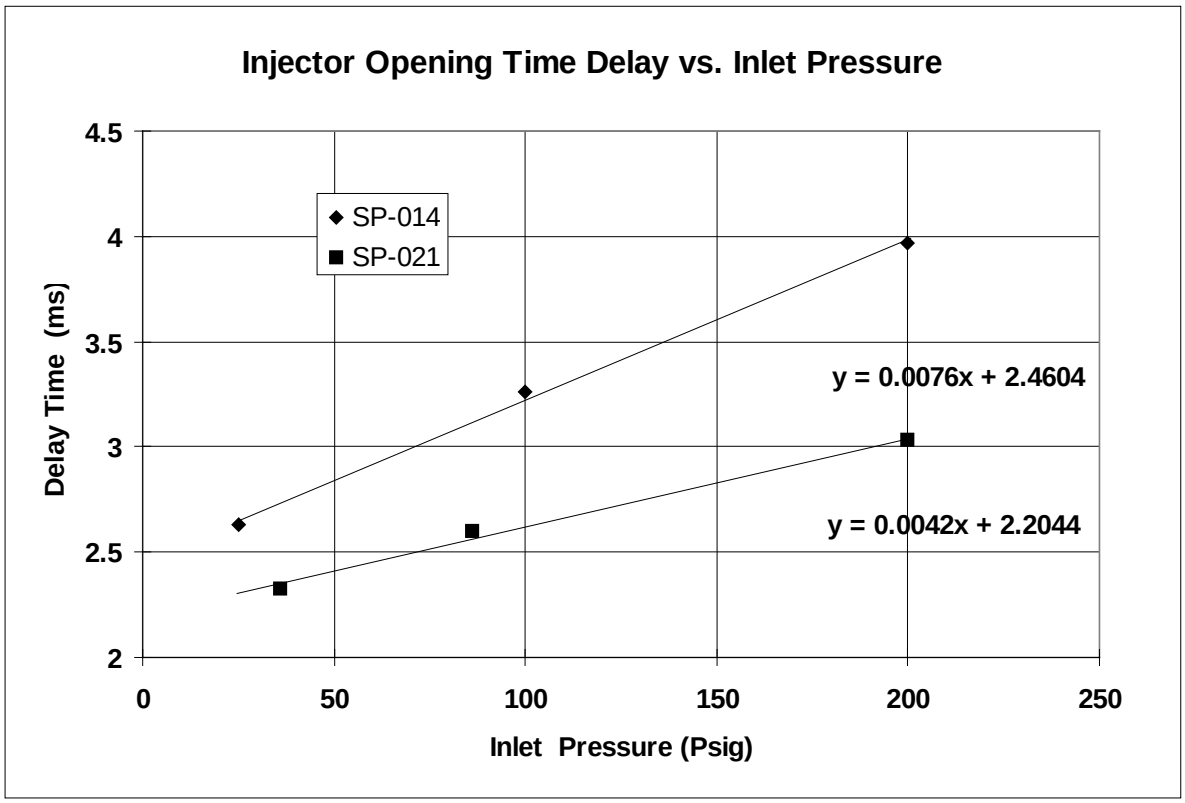

Figure 5-8. Hydrogen fuel leakage rates.

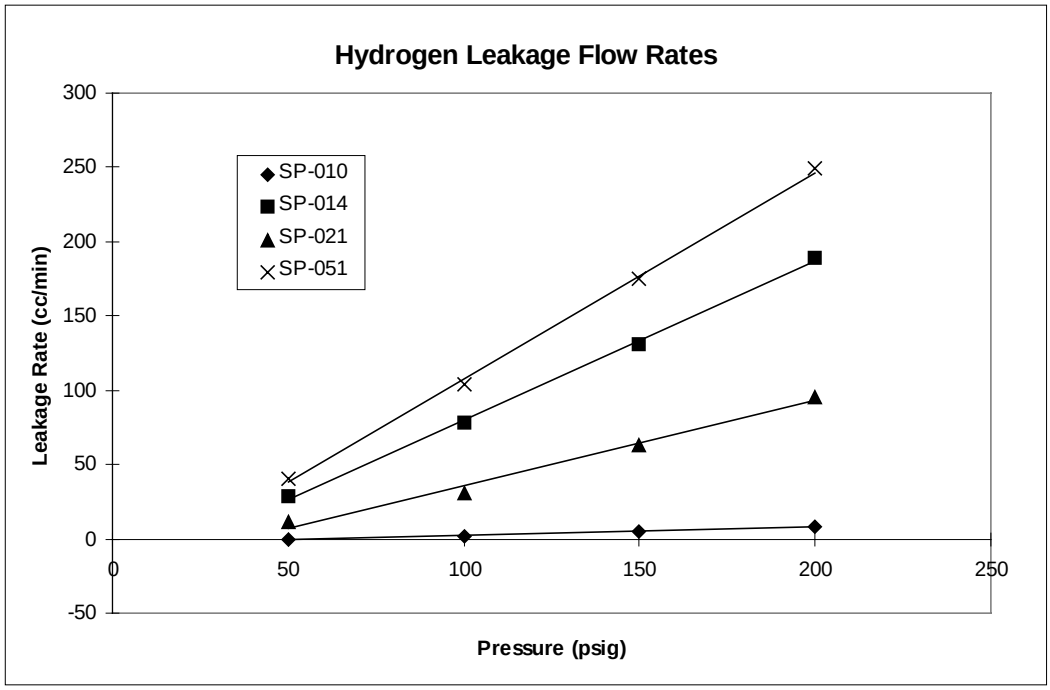

5.4 Battery Balance

Task 6.1 Literature Survey

A review of the literature indicated evidence that lack of battery balancing leads to premature lead-acid battery (battery) failures and loss of charge storage capacity in Series Connected Battery Systems (SCBSs). EV designers have considered the SCBS as a single, two-port device (e.g., Thevenin or Norton equivalent) and charged and discharged it accordingly. However for EV applications, the SCBS is comprised of numerous separate cells; each having a different initial charge storage capacity. The variance of the initial capacity of these cells has not been well quantified. If unaccounted for, these capacity variances will cause overcharging of certain batteries in the SCBS and undercharging in others when using total SCBS voltage to control the charging process—as is the current practice. This progressive process of battery balance degradation will become more prominent as the trend to faster recharge rates continues and as rapid charge cycling (as in HEVs) increases.

Various approaches have been suggested to deal with and/or prevent the unbalanced battery pack problem. Initially choosing the batteries to have the same capacity (e.g., the end user asks for batteries from the same manufacturing lot by the same manufacturer) delays the onset of problems. However, there are several problems with this approach: 1) choosing batteries that have exactly the same capacity is not always feasible; 2) it does not allow for easy replacements of single batteries of the SCBS when the need arises; and 3) it does not deal with the issue of the differential changes occurring in the capacity of each battery as its cycle life progresses.

Hung, Hopkins, and Mosling (1993) suggested individual battery equalization (IBE) by power dissipation, but gave no details on this method. They also suggested an alternate method of power transfer, through the use of separately designed DC to DC step-up converters on each battery, which would return most of the energy to the charger while preventing the battery from reaching an over voltage condition during the charging process. Kutkut (1995) states that this approach was too complicated and expensive, and has suggested a charger be designed that places the batteries in the SCBS in parallel during the final phases of charging through use of a specialized transformer and various feedback systems. This approach would be complicated.

Task 6.2 Design Prototype Battery Bypass Circuit

CE-CERT selected a power dissipation form of IBE to implement. The selection was based on this approach since it was the easiest and least expensive to initially implement (especially for retrofit). CE-CERT has developed a preliminary circuit topology, as shown in **Figure 5-9** with a Bill of Materials given in **Table 5-7**. The circuit is operationally comparable to a precision, high power Zener diode. The idea of the circuits is to allow the charging current to bypass individual batteries in a SCBS as the individual batteries reach their full SOC voltage. With such circuitry, charging could continue until all batteries in the pack attain full charge without overcharging any of the batteries. The circuit uses relatively inexpensive standard electronics with power dissipation occurring in a MOSFET and a set of low-cost, commercial grade power resistors. A patent on this and similar circuits has been filed with the UCR Patent Office.

Figure 5-9. EV battery balancing circuit.

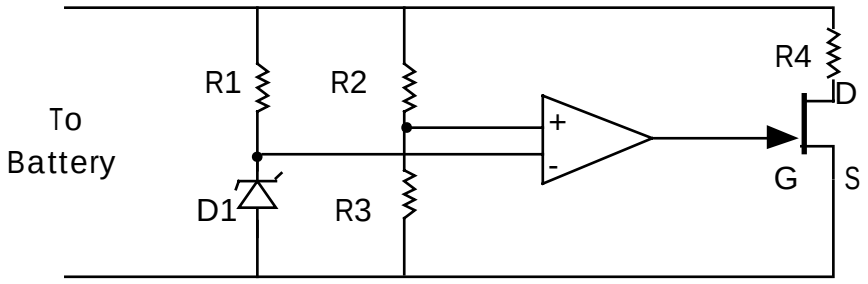

Table 5-7. Battery balance bill of materials.

Description	Part Number	Manufacturer
Mosfet	IRF530N	International Rectifier
Op. Amp.	LM3900	National Semiconductor
Precision Shunt Reg.	LM431ACZ	National Semiconductor
1%, 1/4W Resistors (metal film)	R1 = 5kΩ, R2 = 20kΩ, R3 = 10kΩ	Various
20W Sand Power Resistor	R4 = 3 x .27 Ω (in Series)	Various

Task 6.3 Implement and Test Prototype Battery Bypass Circuit

The circuit of Figure 5-9 has been implemented and lab tested. For this test, the HEV bypass circuit was applied across a 12 volt HEV battery, and charging was simulated by manual control of a 15 volt power supply capable of delivering about 5 amps at 16 volts. Total charging current, voltage across battery terminals, and bypass current were measured at different voltage and current levels. As expected, operation was like a high power, ideal, Zener diode. Ideal implies variable resistance, through the Zener, during Zener controlled operation with the variable resistance adjusting as a function of current to maintain a fixed terminal voltage. For $V_{bat} < V_f$, all charging current is passed through the battery. For $V_{bat} \bullet V_f$, all normal charging current is shunted around the battery by the bypass circuit, but is still available for charging the remaining batteries in the series pack. This allows for efficient, balanced charging of the SCBS without excessive gassing.

Due to the physical properties of the circuitry, if $I_{charge} * R_{power}$ becomes greater that V_f, then the excess current $I_{excess} = I_{charge} - V_f / R_{power}$ will pass through the battery and the battery voltage will continue to rise. (R_{power} is the power dropping resistor shown in Figure 5-9).

Task 6.4 Implement and Test Battery Bypass Circuit on an EV

A thorough evaluation required a battery monitoring system capable of recording individual battery voltages and battery pack current. The monitoring system must present this information

safely to the computer for data acquisition while the EV is in use or being charged. For this purpose, a central, inexpensive, multiplexed, electrically isolated battery monitoring system has been designed. The use of separate inexpensive isolation amplifiers for each battery in the SCBS, in contrast to the previously noted central unit, is being investigated and a prototype is being planned. The use of separate components would allow the IBE and monitoring equipment to be self contained as a stand-alone unit for each battery and makes implementation on various diverse systems relatively easy (again, especially for retrofit purposes).

To provide for controlled testing, IBE bypass circuits were implemented on only half of the vehicle batteries. This allows comparison between bypassed and unbypassed batteries during use. In conjunction with the battery monitoring system, we will be able to monitor the test circuits and control batteries simultaneously. This information, with capacity information, can be used to quantify the process which leads to the unbalanced SOC condition within the battery pack.

Figure 5-10 displays data obtained from on vehicle circuit testing. The bottom curve is the average charging voltage across the batteries with bypassing circuitry. The bypass was designed for V_f = 7.0 V. Note that the measured float voltage of 7.05 V. is within 1% of the design value. The top curve of Figure 5-10 is the average charging voltage across the unbypassed batteries. The average unbypassed charging voltage exceeds the specified float voltage by up to 0.5 V. This figure demonstrates proper battery bypass operation. Long-term battery monitoring is required to determine if the batteries with the bypass circuitry outlast those without the bypass circuit.

5.5 Energy Management

Since an HEV has multiple sources of electrical energy (e.g., batteries, APU), strategies are necessary to specified how to best satisfy the instantaneous power demand from the various sources. Under this task, CE-CERT has designed, developed, and evaluated different energy management strategies for use in HEVs.

Task 7.1 Literature Survey

The objective of the energy management system is to meet the drivetrain power requirements while minimizing fuel usage and emissions. A detailed review of existing energy management techniques for series HEVs has been completed and is reviewed below.

The spectrum of energy management strategies for series HEVs can be well illustrated by considering the two extreme strategies of constant power (thermostatic) and load following. For most vehicles, the optimal strategy will require some compromise between these two strategies.

Figure 5-10. Average charging voltage for unbypassed batteries (top curve) and bypassed batteries (bottom curve)

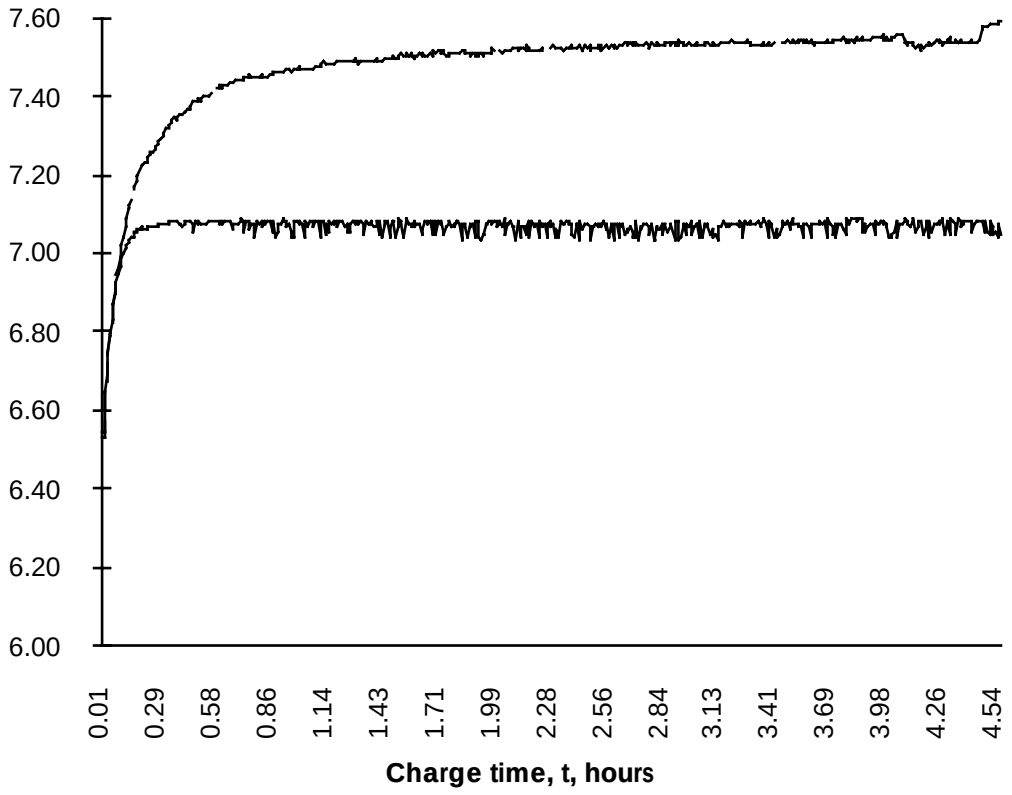

Thermostat switching is the most commonly used energy management strategy. It is motivated by the following: 1) the APU is most efficient and cleanest at constant speed and full design power; and 2) battery losses increase dramatically at extreme SOC values. With these motivations, the APU is cycled much like the thermostat in a building. The HEV is run in EV mode until the batteries achieve a threshold minimum SOC denoted by α. Once SOC(t) < α, the APU turns on and is regulated to run at its most efficient speed. Since by design, this power level will exceed the average drivetrain power requirement, the battery SOC will tend to increase. Once the SOC achieves some upper limit denoted by β, the APU turns off. By proper choice of α and β (typical values for α and β are 10% and 90% respectively), extreme SOC levels will normally be avoided—extending battery life, minimizing losses, and ensuring drivability. By running the APU in this manner, fuel usage and pollutant emissions are minimized. Drawbacks of this approach include: 1) the possibility of the SOC(t) < α condition being achieved just prior of a situation requiring peak power; 2) the possibility of the SOC(t) > β condition being attained just prior to a regenerative opportunity; 3) the necessity for catalyst preheating, since the intervals between APU usage will normally be sufficiently long as to allow the catalyst to cool; and 4) high battery losses, since the strategy cycles all energy into and out of the battery before using it for propulsion.

Load following strategies are motivated by the desire to minimize the transmission of energy through the batteries (due to high round trip losses) and to use the batteries only in their optimal SOC range. For typical lead acid batteries, this range would be 40% < SOC(t) < 70%. In this strategy, the HEV is used in a pure EV mode until SOC(t) ε [α,β]. Within this range the APU is turned on with the objective of providing as nearly as possible the drivetrain power requirements. Therefore, the batteries in this SOC range are acting only as a load leveling device (i.e., not a net source of energy). Round trip battery losses are minimized, since the majority of energy does not pass through the batteries; however, the APU efficiency is decreased and emissions increased as the APU does not operate at its optimal speed and its output power level must follow rapid transients.

Optimized strategies will tradeoff the characteristics and benefits of these two approaches.

Task 7.2 Modeling and Simulation Evaluation

Based on the outcome of the literature search, an HEV simulation was constructed to implement and comparatively evaluate alternative energy management strategies. The simulation is general enough to allow evaluation and design of energy management strategies for various HEVs. All evaluations performed relative to this project were for the CE-CERT HEVT.

For each major component of an HEV, we have evaluated its effect on overall energy management and any special constraints that it imposes on the energy management strategy. We have created a simulation model for testing of several different energy management strategies. The simulation is based on a systems model shown in **Figure 5-11.**

The dynamic equations corresponding to each component of Figure 5-11 have been documented in Farrell and Barth (1997) . This article also discusses several important issues related to energy management.

Figure 5-11. Overall system model.

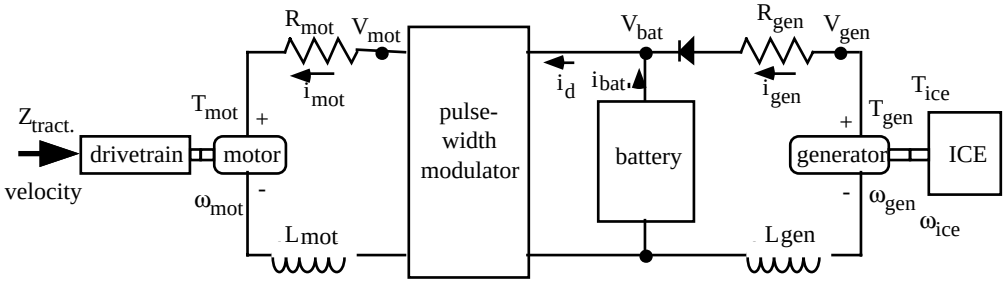

The system of ordinary differential equations is integrated with a variable step-size Runga-Kutta algorithm. An example output of our simulation for an open-loop strategy is given in **Figures 5-12a, b, and c** during thermostatic energy management. Note that the stated objective for thermostaic control of running the APU "at constant power" is not met on a continuous basis. This is true since the generator and ICE dynamics limit the maximum and rate of change of the

ICE power and the generator current. Even if the generator current could be held constant, changes in the bus voltage due to the time varying motor current would cause the APU power output to be non-constant.

7.3 HEV Energy Management Design

The optimal energy management strategy for a given HEV will normally lie somewhere between the thermostatic and load following strategies described above. CE-CERT has designed and tested in simulation an energy management strategy designed specifically for the HEVT. The design work has included architecture definition (Figure 5) and infrastructure (sensing and data acquisition) requirements.

The block diagram in Figure 5 displays the various components of the energy conversion processes onboard a series HEV. The bold lines indicate energy flow with directionality indicated by arrowheads. The dashed lines indicate the flow of information and control signals. The narrow solid lines indicate the accelerator and brake linkages. In addition to the indicated control signals, the electric drivetrain and power source are assumed to have internal control systems.

The block diagram shows the various variables monitored by the energy manager to accurately estimate current power requirements, and current battery state of charge. Using this information, the energy manager is responsible for monitoring energy usage and power requirements to ensure that the expected power requirements can be met. The ability to meet anticipated power requirements depends on both the power generation capability and the ability to accurately predict power requirements.

Figure 5-12a. ICE output power for the thermostatic strategy α = .2, β = .8

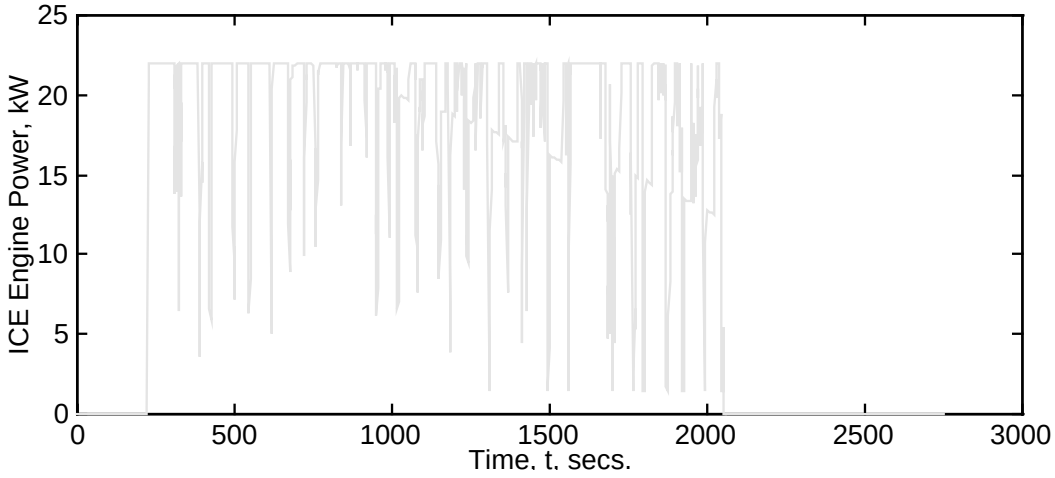

Figure 5-12b. Battery SOC for the thermostatic strategy, α = .2, β = .8

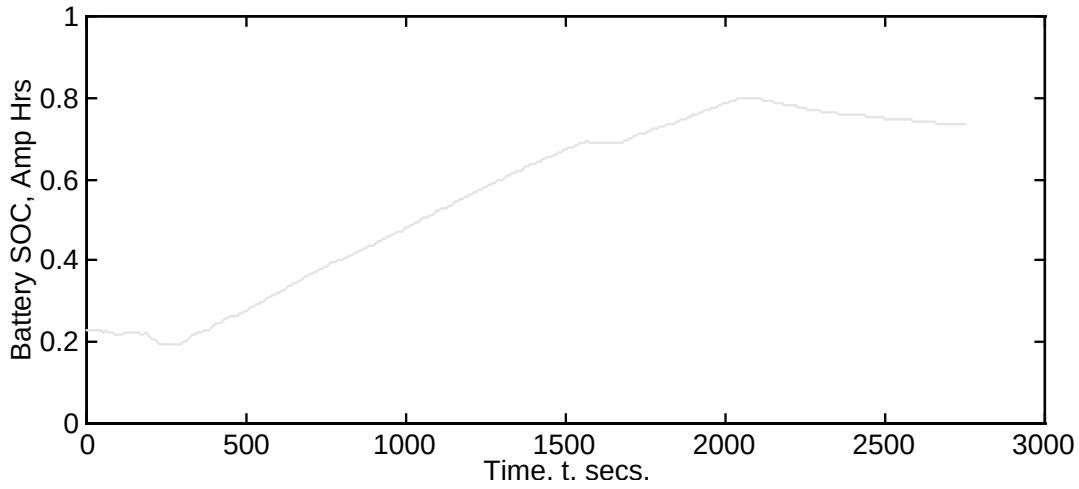

Figure 5-12c. Battery output power for the thermostatic strategy, α = .2, β = .8

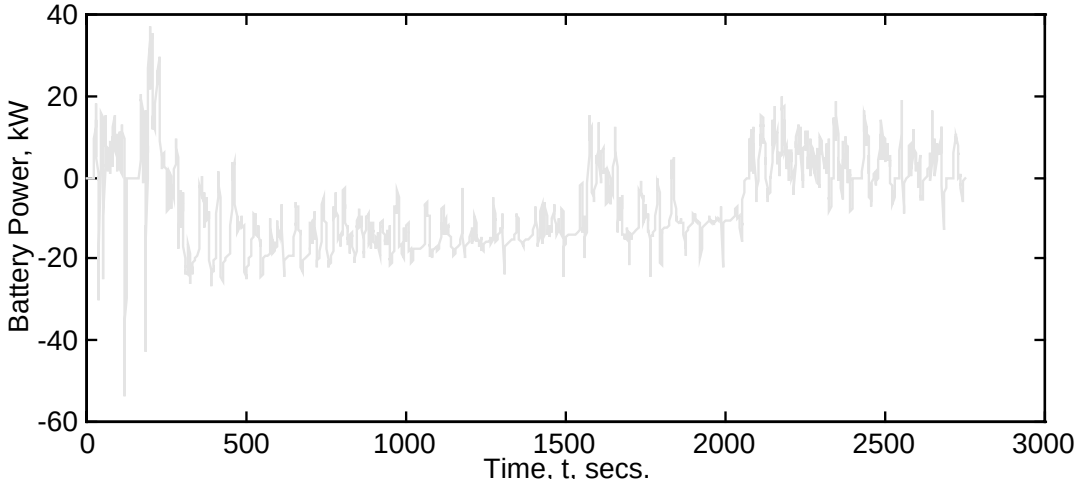

Figure 5-13. Schematic of HEV energy conversion processes.

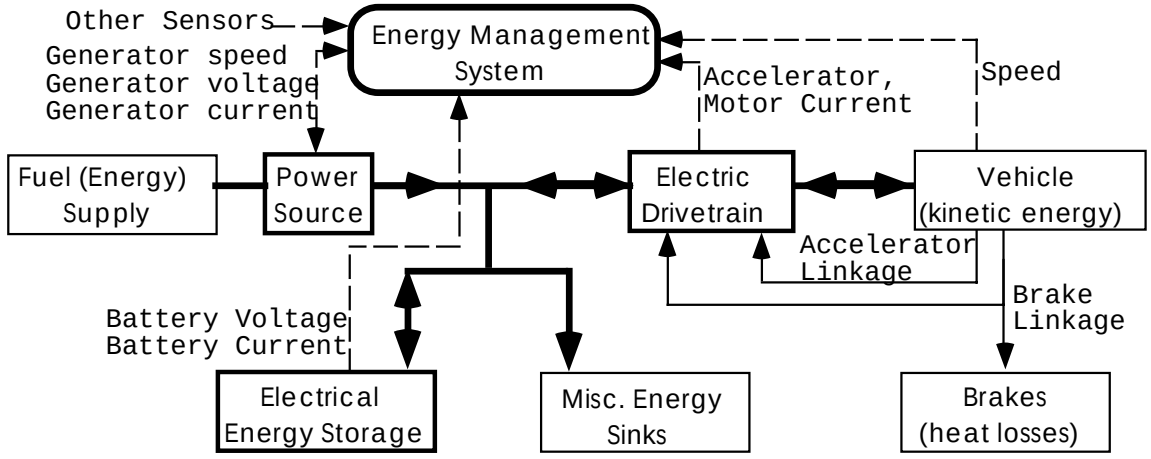

The designed energy management strategy is a compromise between the two extreme strategies described above to achieve the key advantages of both techniques. For example, given that the battery charge and discharge efficiencies are e_c and e_d then for a drivetrain power requirement p(t), the APU would have to supply p(t) in a perfect load following mode or $\frac{p(t)}{e_c\, e_d}$ in a thermostat strategy with all the APU power cycling through the batteries. Obviously, it is more efficient to supply the power directly. This analysis does not however describe the complete picture, as the ICE efficiency drops off rapidly as the ICE output power decreases and the emissions increase substantially during power transients.

Therefore, a compromise strategy with the following features should perform better than either of the two extreme strategies:

1) For SOC > β, the HEV drives in a pure EV mode.
2) For α < SOC < β, the HEV drives in a limited (see below) load following mode.
3) For α • SOC, the HEV drives in a operates in a high power mode.
4) If power demand can be accurately predicted, then the HEV would revert to a pure EV mode once the energy requirements for the remainder of the trip could be achieved from the current HEV battery SOC.

Limited load-following refers to the APU output power following the drivetrain power requirements subject to limitations on the rate of change of the APU output power (to minimize emissions) and on the minimum APU power output (to maintain high ICE efficiency). The load-following command is specified by the energy manager as a commanded current. The APU output power would slightly exceed the rate limited drivetrain power requirements when SOC is near the lower edge of the range specified in 2) and be slightly less than the rate limited drivetrain requirements when SOC is near the upper edge of the range specified in 2). The objective is to regulate SOC about the battery's most efficient point of operation. The battery SOC will not remain constant, as the batteries are meeting the transient drivetrain power

requirements that the rate and power limited APU does not achieve; however, the peak battery currents will be greatly decrease, since the generator current will follow the average drivetrain requirement.

Task 7.4 Energy Management Implementation and Testing

The HEV APU and DAQ system are being developed under other contracts. In this project, implementation of the energy management system was addressed only to the ensure that the work done for the other contracts would result in systems compatible with the future objectives of this project.

The three strategies described above have been implemented and tested in simulation. The results are meant to demonstrate typical performance of each strategy. The objective of these examples is not to demonstrate which strategy is 'best', as this evaluation is dependent on the vehicle under study, the driving profile, and specifics of the energy management strategy.

It is important, however, to note that the energy management strategy must be carefully designed. **Table 5-8**, for example, shows the total fuel requirements and CO emissions for each of the three strategies. The actual magnitude of the numbers is not important and should not be considered typical for any HEV (since the simulated vehicle was not optimized in anyway). The main point is that for the given vehicle, significant fuel usage and CO emission reductions are possible just by careful designing of the energy management system.

Table 5-8. Fuel usage (corrected for end SOC) and CO emissions for the simulated vehicle using different strategies over identical simulation runs.

Strategy	Fuel (total kJ)	CO (total grams)
Thermostatic	104907	31.4512
Load-Following	67780	19.2121
Optimized	47500	13.1

6.0 Conclusions and Recommendations

Tests results indicate that the sonic flow, pulse-width-modulated electronic injectors for gaseous fuels used in this project provided precise, stable and reliable metering of hydrogen gas. This is evident in the linear flow curves during wide open operation and in the low standard deviation error during pulse-width-modulation shown in Tables 5-1 to 5-4.

Table 6-1 and 6-2 list the throughput (mg of hydrogen/injector) for each injector for the design requirements of 4.83 ms (variable speed engine) and 6.90 ms (constant speed engine), respectively. It can be seen from Table 6-1 that the SP-010 is capable of meeting the requirement of 8.4 mg of hydrogen per injection for the variable speed engine. For the constant speed engine, Table 6-2 indicates that all of the injectors are capable of meeting the design requirement of 6.9 mg of hydrogen per injection.

Although the performance and durability of these injectors were excellent for these limited tests, the question of long-term durability using hydrogen has not been fully addressed. It is recommended that further testing, preferably on an operating engine, be conducted to address this issue.

CE-CERT is fabricating the smaller of these two engines (the hydrogen-fueled APU) for installation in a hybrid-electric vehicle.

A battery bypass circuit was designed, developed, and applied on a set of lead-acid batteries, currently in use on an electric vehicle. Controlled testing was performed, showing that the circuit functions properly in not overcharging the batteries when the battery pack is unbalanced.

Further, we have described the critical components of an HEV and how their characteristics relate to the HEV's energy management strategy. For batteries, a critical characteristic in the strategy design is the low round-trip efficiency and its dependence on the state-of-charge. For the APU, fuel economy, emissions, and to a lesser extent noise are the critical issues. The examples of Section 5.5 demonstrate the importance of carefully analyzing and designing the energy management systems and the utility of a dynamic HEV simulation. The design of state-of-the-art energy managers has a profound effect on the fuel economy and emissions.

Open-loop energy management has two main drawbacks:

1. APUs usually are sized for a selected average power requirement. An open-loop energy management strategy could result in a low battery state-of-charge in a predictable situation where a high state-of-charge is desirable (e.g., at the bottom of a steep hill) or a high state of charge when a significant regenerative braking opportunity arises.

2. With aging effects on the APU, utility emissions associated with charging the HEV's energy storage system are typically less than the emissions of the APU. Therefore, it is desirable to minimize the use of the APU in order to minimize overall emissions, particularly when operating in areas of non-attainment, such as the South Coast Air Basin.

Table 6-1. Hydrogen flow at a PW of 4.83 ms (requirement for the variable speed engine)

SP-014 at 200 psig						
Engine Speed (RPM)	1000	2000	3000	4000	5000	6000
Time for one Rev (ms/rev)	60	30	20	15	12	10
Injection Duration (°)	145	145	145	145	145	145
Flow Time (PW) for 145° (ms)	24.2	12.1	8.1	6	4.8	4
PW to achieve required flow time (ms)	26.3	14.2	10.2	8.1	6.9	6.1
Mass of H_2 per Injection (mg/inj)	36.9	19.7	14	11.2	9.5	8.3
Volume of Hydrogen /injection (c.i.)	27.46	14.7	10.44	8.32	7.04	6.19
Volume per cylinder (c.i.)	183	98	70	55	47	41
Engine Displacement						
4 cylinder	732	392	278	222	188	165
6 cylinder	1098	588	418	333	282	248
8 cylinder	1465	784	557	443	**375**	330
10 cylinder	1831	980	696	554	469	413
12 cylinder	2197	1176	835	665	563	495
SP-021 at 200 psig						
Engine Speed (RPM)	1000	2000	3000	4000	5000	6000
Time for one Rev (ms/rev)	60	30	20	15	12	10
Injection Duration (°)	145	145	145	145	145	145
Flow Time (PW) for 145° (ms)	24.2	12.1	8.1	6	4.8	4
PW to achieve required flow time (ms)	25.6	13.5	9.5	7.4	6.2	5.4
Mass of H_2 per Injection (mg/inj)	28.2	14.6	10	7.8	6.4	5.5
Volume of Hydrogen /injection (c.i.)	21.02	10.86	7.48	5.78	4.77	4.09
Volume per cylinder (c.i.)	140	72	50	39	32	27
Engine Displacement						
4 cylinder	561	290	199	154	127	109
6 cylinder	841	434	299	231	191	164
8 cylinder	1121	579	399	308	**254**	218
10 cylinder	1401	724	498	386	318	273
12 cylinder	1682	869	598	463	381	327

Open-loop energy management may result in a near fully charged battery pack at trip end. Therefore, there would be significant advantages to the development and implementation of advanced, predictive energy management strategies. Advanced energy management systems using adaptive and positioning techniques could further improve HEV performance. The development of advanced energy management systems is currently only at a preliminary stage and should be investigated in future research.

Table 6-2. Hydrogen flow at a PW of 6.90 ms (requirement for the constant speed engine)

Inlet Pressure (psig)	SP-014 (mg/inj)	SP-021 (mg/inj)	SP-051 (mg/inj)	SP-010 (mg/inj)
25	1.82	1.82	-	-
50	4.08	2.97	2.45	10.17
75	5.65	3.82	-	-
100	6.53	4.76	4.18	14.99
125	7.12	5.28	-	-
150	7.93	6.00	5.52	-
175	8.99	7.26	-	-
200	10.17	8.43	7.19	-

7.0 References

Barkhimer, R.L.; Beck, N.J.; and Weseloh, W.E. (1983). Development of a Durable, Reliable and Fast Responding Solenoid Valve. SAE Paper 831326. Warrendale, PA.

Barkhimer, R.L., and Wong, H. (1995). Application of Digital, Pulse-Width-Modulated Sonic Flow Injectors for Gaseous Fuels. SAE Paper 951912. Also in *Gaseous-Fuel Engine Technology* SAE SP-1104. Warrendale, PA.

BKM, Inc. (1996). Information provided by BKM with the purchase of natural gas injectors.

Cecil, W. (1822). On the Application of Hydrogen Gas to Produce a Moving Power in Machinery; with a Description of an Engine which is Moved by the Pressure of the Atmosphere, upon a Vacuum Caused by Explosions of Hydrogen and Atmospheric Air. *Trans. Cambridge Philos. Soc.*, **1**:217.

Das, L.M. (1990). Hydrogen Engines: A View of the Past and a Look into the Future. *Int. J. Hydrogen Energy*, 15:6, pp. 425-443.

Dickinson, B., and Swan, D. (undated). EV Battery Pack Life: Pack Degradation and Solutions,, pp. pp. 145-153.
Farrell, J., and Barth, M. (1997). Simulation/Evaluation of Series Hybrid Electric Vehicle Performance. *Proc. 1997 World Car Conference*, pp. 567-582. Riverside, CA.

Giannacopoulos, T., et. al. (1986). Preliminary Investigations on a Microprocessor Controlled Gaseous Hydrogen Injector. *Computers in Engineering*, Proceedings of the 1986 ASME International Computers in Engineering Conference and Exposition, Chicago, July 20-24.

Glasson, N.D., and Green, R.K. (1994). Performance of a Spark-Ignition Engine Fueled with Hydrogen Using a High-Pressure Injector" *Int. J. Hydrogen Energy* **19**:917-923.

Hall, J. V., et al. (1992). Valuing the Health Benefits of clean air. *Science*, Vol.. 255, pp. 812-817.

Hoffmann, P. (1981). *The Forever Fuel: The Story of Hydrogen.* Westview Press, Boulder, CO.

Homan, H.S., et. al. (1983). The Effect of Fuel Injection on NOx Emissions and Undesirable Combustion for Hydrogen-Fueled Piston Engines. *Int. J. Hydrogen Energy* **8**:131-146.

Hung, S.; Hopkins, D.; et al. (1993). Extension of Battery Life via Charge Equalization Control. *IEEE Trans. on Ind. Elect.*, 40:96-104.

King, R.O., and Allan, A.B. (1955). The Oxidation, Decomposition, Ignition and Detonation of Fuel Vapors and Gasses: XXIX. The Role of Nuclei in the Ignition by Compression of Gaseous

Heptane-Air Mixtures: First paper. *Canadian Journal of Technology*, **34**:316-334, 1956. Also see R.O. King and M. Rand, XXVII. The Hydrogen Engine, Op. Cit. **33**:445-469.

Koyanagi, K., et. al. (1994). Study on Mechanism of Backfire in Hydrogen Engines. SAE Paper 942035. Warrendale, PA.

Kutkut, N.H.; Wiegman, H.L.N.; et al. (1995). Design Considerations for Charge Equalization of an Electric Vehicle Battery System. Tenth Annual Applied Power Electronics Conference and Exposition, pp. 96-103.

Lynch, F.E. (1983). Parallel Induction: A Simple Fuel Control Method for Hydrogen Engines, *Int. J. of Hydrogen Energy*, **8**:721.

MacCarley, C.A., and Van Vorst, W.D. (1980). Electronic Fuel Injection Techniques for Hydrogen Powered I.C Engines. *Int. J. Hydrogen Energy* **5**:179-203.

Norbeck, J.M., et. al. (1996). *Hydrogen Fuel for Surface Transportation*, Society of Automotive Engineers, Inc., Warrendale, PA.

Oehmichen, M. (1942). Wasserstoff als Motortreibmittel. In Deutshche Kraftfahrtforschung, 68, VDI-Verlag GMBH, Berlin.

Swain, M.R., et. al. (1983). Hydrogen Engine Data-base Summary. SAE Paper 839089. Warrendale, PA.

South Coast Air Quality Management District (1994). *Air Quality Management Plan*. Diamond Bar, CA. September.

Varde, K.S., and Frame, G.M. (1985). A Study of Combustion and Engine Performance Using Electronic Hydrogen Fuel Injection. *Int. J. Hydrogen Energy* 9:327-332. Also see Development of a High-Pressure Hydrogen Injection for SI Engine and Results of Engine Behavior, *Int. J. Hydrogen Energy* **10**:743-748.

Wang, Q.; DeLuchi, M.; et al. (1990). Emission Impacts of Electric Vehicles. *J. Air & Waste Management Assn.*. 40:1275-1284.